RNase P protein subunit Rpp29 represses histone H3.3 nucleosome deposition

Alyshia Newhart[a], Sara Lawrence Powers[a], Prashanth Krishna Shastrula[a,b], Isabel Sierra[a], Lucy M. Joo[a], James E. Hayden[a], Andrew R. Cohen[c], and Susan M. Janicki[a,*]

[a]Molecular and Cellular Oncogenesis Program, Wistar Institute, Philadelphia, PA 19104; [b]Department of Biological Sciences, University of the Sciences in Philadelphia, Philadelphia, PA 19104; [c]Electrical and Computer Engineering Department, Drexel University, Philadelphia, PA 19104

ABSTRACT **In mammals, histone H3.3 is a critical regulator of transcription state change and heritability at both euchromatin and heterochromatin. The H3.3-specific chaperone, DAXX, together with the chromatin-remodeling factor, ATRX, regulates H3.3 deposition and transcriptional silencing at repetitive DNA, including pericentromeres and telomeres. However, the events that precede H3.3 nucleosome incorporation have not been fully elucidated. We previously showed that the DAXX-ATRX-H3.3 pathway regulates a multi-copy array of an inducible transgene that can be visualized in single living cells. When this pathway is impaired, the array can be robustly activated. H3.3 is strongly recruited to the site during activation where it accumulates in a complex with transcribed sense and antisense RNA, which is distinct from the DNA/chromatin. This suggests that transcriptional events regulate H3.3 recruited to its incorporation sites. Here we report that the nucleolar RNA proteins Rpp29, fibrillarin, and RPL23a are also components of this H3.3/RNA complex. Rpp29 is a protein subunit of RNase P. Of the other subunits, POP1 and Rpp21 are similarly recruited suggesting that a variant of RNase P regulates H3.3 chromatin assembly. Rpp29 knockdown increases H3.3 chromatin incorporation, which suggests that Rpp29 represses H3.3 nucleosome deposition, a finding with implications for epigenetic regulation.**

Monitoring Editor
Susan Strome
University of California, Santa Cruz

Received: Feb 27, 2015
Revised: Jan 25, 2016
Accepted: Jan 28, 2016

INTRODUCTION

Unlike the canonical histones, which are incorporated into nucleosomes coincident with DNA replication, the histone H3 variant H3.3 is synthesized throughout the cell cycle and used for replication-independent (RI) chromatin assembly (Talbert and Henikoff, 2010). The RI incorporation of H3.3 into nucleosomes occurs at both euchromatin and heterochromatin and is regulated by at least two independent chaperoning systems. The HIRA/Cabin1/Ubinuclein-1/Asf1a complex mainly regulates genic deposition (Filipescu *et al.*, 2013). The H3.3 chaperone death-domain–associated protein (DAXX), together with the chromatin-remodeling factor α-thalassemia/mental retardation syndrome X-linked (ATRX), regulates H3.3 chromatin assembly and transcriptional silencing at repetitive regions, including pericentromeres (Drane *et al.*, 2010), telomeres (Goldberg *et al.*, 2010; Wong *et al.*, 2010), endogenous retroviruses (Elsasser *et al.*, 2015; He *et al.*, 2015; Sadic *et al.*, 2015), differentially methylated regions, and intragenic methylated CpG islands (Voon *et al.*, 2015). Although RI H3.3 chromatin assembly is highly conserved, its essential function is incompletely understood, and events upstream of nucleosome deposition remain largely undefined.

In mammals, RI H3.3 chromatin assembly regulates genome plasticity and transcription state heritability. In embryonic stem cells (ESCs), the promoters of developmentally regulated genes are typically enriched with both H3 K4 trimethylation (H3K4me3) and H3 K27 trimethylation (H3K27me3), histone posttranslational modifications (PTMs) associated with gene activation and silencing, respectively (Bernstein *et al.*, 2006). However, in the absence of HIRA-mediated H3.3 incorporation, H3K27me3 fails to become established

This article was published online ahead of print in MBoC in Press (http://www.molbiolcell.org/cgi/doi/10.1091/mbc.E15-02-0099) on February 3, 2016.

*Address correspondence to: Susan M. Janicki (sjanicki@wistar.org).

Abbreviations used: AS, antisense; ATRX, α-thalassemia/mental retardation syndrome X-linked; DAXX, death-domain–associated protein; ESC, embryonic stem cell; PTM, posttranslational modification; RC, replication coupled; RI, replication independent; S, sense.

at these "bivalent" promoters, and gene expression is dysregulated during differentiation (Delbarre *et al.*, 2010; Goldberg *et al.*, 2010; Yang *et al.*, 2011; Banaszynski *et al.*, 2013). H3.3 is also required for H3K9me3 at DAXX-ATRX–mediated sites (Elsasser *et al.*, 2015; He *et al.*, 2015; Jang *et al.*, 2015; Udugama *et al.*, 2015; Voon *et al.*, 2015). Its enrichment at ESC telomeres and the decrease in its incorporation that follows differentiation suggest that H3.3 functions to maintain transcriptional silencing before telomeres are converted into constitutive heterochromatin (Wong *et al.*, 2009, 2010; Goldberg *et al.*, 2010).

H3.3 is also required for the de novo establishment of chromatin domains. In zygotes, H3.3 regulates the changeover of the male genome from protamines to nucleosomal histones and the assembly of centric and pericentric DNA into constitutive heterochromatin (Loppin *et al.*, 2005; Torres-Padilla *et al.*, 2006; Santenard *et al.*, 2010). During the latter process, the maternal and paternal pericentric DNA, as well as DAXX, ATRX, and H3.3, localize in rings around nucleoli, suggesting that their nucleolar association is functionally important (Martin *et al.*, 2006; Probst *et al.*, 2007). Indeed, when oocytes are enucleolated, DAXX is mislocalized, centric and pericentric DNA is depleted, and embryos arrest at the two-cell stage (Fulka and Langerova, 2014). This suggests that nucleolar proteins are required for the DAXX-ATRX-H3.3–mediated assembly of pericentric DNA into heterochromatin that follows fertilization. However, their identity and functions are unknown.

Because the majority of the histone proteins in the cell are nucleosomal, one of the biggest challenges to deciphering upstream regulatory events is identifying the factors that H3.3 interacts with before chromatin incorporation. We reported that DAXX and ATRX regulate both H3.3 deposition and transcriptional silencing at a multicopy array of an inducible reporter construct that can be visualized in single-living cells (Newhart *et al.*, 2012). When the DAXX-ATRX-H3.3 pathway is impaired, the array can be rapidly and robustly activated. Of interest, H3.3 is still recruited to the site, where it associates with sense and antisense RNA transcribed from the transgene in a complex that is distinct from the DNA/chromatin (Newhart *et al.*, 2013b). Therefore we identified an experimental system in which H3.3 can be visualized in association with its incorporation site at a step upstream of nucleosome deposition. Using this system, we identified the nucleolar RNA proteins Rpp29, fibrillarin, and RPL23a as components of this H3.3/RNA complex. Rpp29 knockdown increases H3.3 chromatin incorporation, which suggests that it functions to repress H3.3 chromatin assembly. A comprehensive understanding of the mechanisms that regulate H3.3 chromatin assembly could provide new insight into how H3.3 regulates the establishment of heritable transcription states.

RESULTS

Single-cell imaging system for evaluating transcriptional dynamics at a DAXX-ATRX-H3.3–regulated chromatin site

To create a system for studying transcriptional dynamics in single living cells, we engineered an inducible reporter construct to include arrays of the lac operator and MS2 RNA stem-loop sequences, which allow simultaneous visualization of DNA and RNA at a transcription site (Janicki *et al.*, 2004; Figure 1A). Transcription is induced by binding of a tetracycline-responsive activator to the tetracycline response elements (TREs) and driven from the minimal cytomegalovirus (CMV) promoter. The mRNA encodes cyan fluorescent protein (CFP) fused to a peroxisomal targeting signal (SKL), the MS2 repeats, and the rabbit β-globin intron 2 splicing module and 3′ untranslated region. The transgene was stably integrated into cells, and clonal lines with multicopy integrations (several hundred copies) in single genomic locations were isolated and used for these studies (Tsukamoto *et al.*, 2000; Janicki *et al.*, 2004; Newhart *et al.*, 2012).

The transcription unit in the transgene is activated using an engineered version of the tetracycline transcriptional activator (tTA) that is composed of the VP16 transcriptional activation domain fused to the TRE-binding domain, which associates with the TREs in the absence of tetracycline (Newhart and Janicki, 2014). We fused tTA to both Cherry and the estrogen-receptor hormone-binding domain (ER) to create Cherry-tTA-ER, which is retained in the cytoplasm until 4-hydroxytamoxifen (4-OHT) triggers it to enter the nucleus, where it accumulates at the array and activates transcription. Cherry-tTA-ER binds directly to the TRE repeats, which permits direct visualization of the active array. The reverse tet transcriptional activator (rtTA), which binds in the presence of doxycycline (Dox), can also be used to activate transcription. The MS2 protein binds to the MS2 RNA stem-loops and is used to visualize the transcribed RNA. The appearance of the CFP-SKL protein in the cytoplasm confirms that the steps required for gene expression have been completed.

The DAXX-ATRX pathway regulates H3.3 chromatin assembly and transcriptional silencing at the transgene array

It was previously shown that the presence of multiple homologous copies of a transgene within a concatameric array can have repressive effects on gene expression in mammalian systems (Garrick *et al.*, 1998; McBurney *et al.*, 2002). However, the mechanisms through which transgene arrays are transcriptionally silenced in mammalian cells have not been fully elucidated. We previously showed that the DAXX/ATRX/H3.3 pathway regulates silencing at the transgene array in our experimental system (Supplemental Figure S1). In HeLa cells, which express both DAXX and ATRX, the array is refractory to activation, and H3.3 is enriched in the chromatin (Newhart *et al.*, 2012). In contrast, arrays integrated into ATRX-null U2OS cells can be robustly activated (Rafalska-Metcalf *et al.*, 2010). During activation, H3.3 is strongly recruited to the site, where it accumulates with transcribed sense (S) and antisense (AS) RNA in a complex that is distinct from the DNA/chromatin. This suggests that the H3.3 at the activated array in the U2OS cell line is arrested at a step before nucleosome deposition (Newhart *et al.*, 2013b). Therefore the U2OS cell line can be used to identify factors that interact with H3.3 upstream of nucleosome incorporation and the HeLa cell line to evaluate their functions in H3.3 chromatin assembly and transcriptional silencing. The regulatory characteristics of the transgene arrays in the HeLa and U2OS cell and the figures in which each cell line is used are summarized in Supplemental Figure S1.

H3.3 N-terminal sequences target it to nucleoli

To identify events that occur upstream of H3.3 nucleosome deposition, we first characterized the localization dynamics of newly synthesized H3.3 in the U2OS cell line. To do this, we transfected the activator Cherry-tTA-ER in combination with yellow fluorescent protein (YFP)–tagged full-length H3.3 and the deletion construct, H3.3-N-tail-αN (Figure 1B), and evaluated their localization patterns 18 and 48 h later. We previously showed that sequence elements in this H3.3 N-terminal construct are sufficient for H3.3 recruitment to the activated array (Newhart *et al.*, 2013b). It was also previously reported that newly synthesized H3.3 accumulates in nucleoli (Delbarre *et al.*, 2012). Here we show that 18 h posttransfection, H3.3 is enriched in nucleoli, as well as at the activated array, in the majority of cells (Figure 1, C, a–c [arrowheads in a indicate nucleoli], and D). We also reported that the recruited H3.3 does not completely colocalize with the activator Cherry-tTA-ER but is instead in a

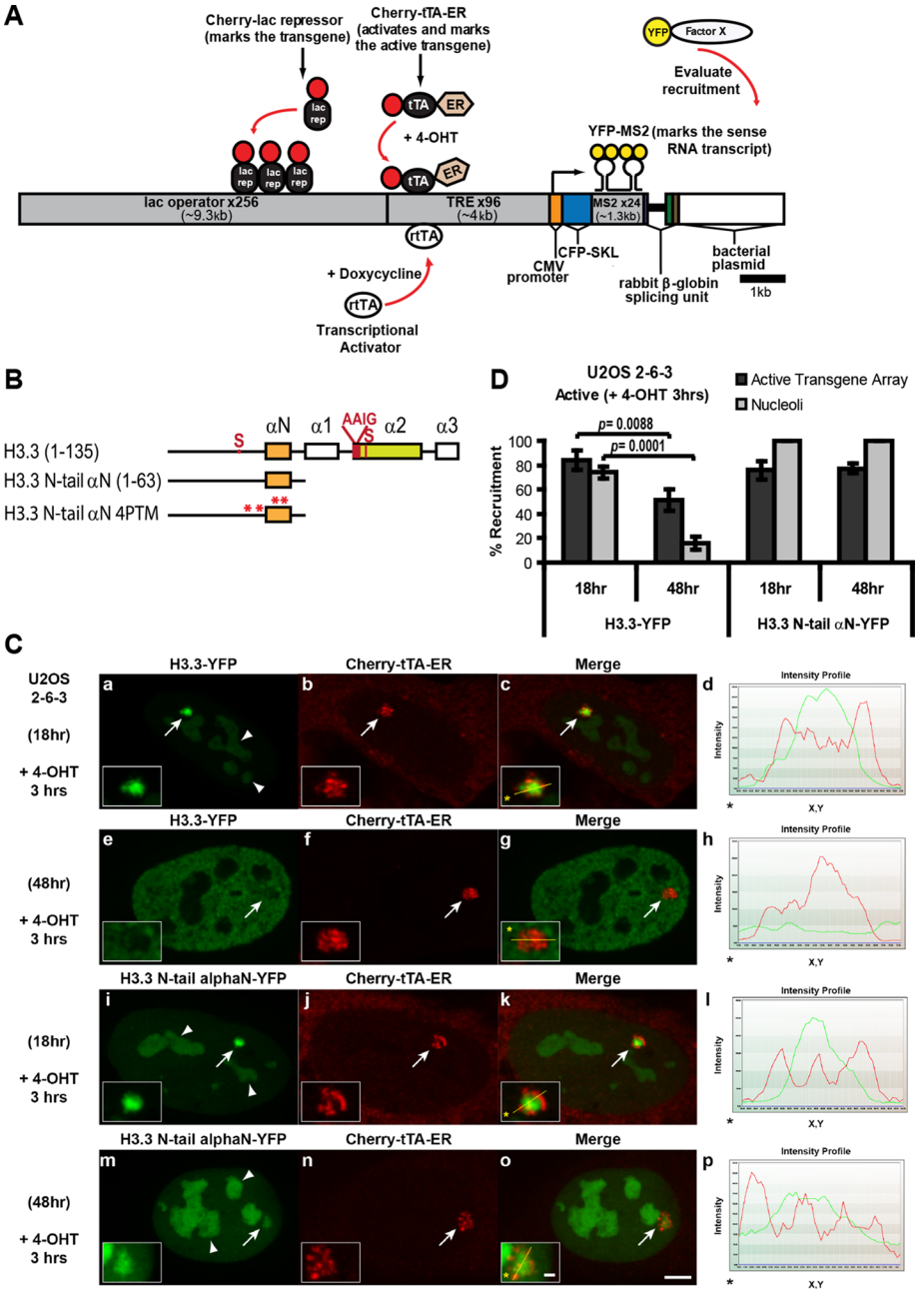

FIGURE 1: Histone H3.3 is enriched in nucleoli before being incorporated into chromatin. (A) Diagram of the inducible transgene drawn to scale. Cherry-lac repressor allows the transgene integration site to be visualized. Transcription is induced from the minimal CMV promoter by the activators Cherry-tTA-ER (+)4-OHT and rtTA (+)Dox. The transcribed RNA encodes CFP fused to a peroxisomal targeting signal (SKL). The RNA is visualized by YFP-MS2, which binds to the stem-loops in the transcript. The 3′ end of the transcription unit is composed of the intron 2 splicing unit from the rabbit β-globin gene. The recruitment of YFP-tagged factors to the array can be monitored by coexpression with the DNA- and RNA-binding proteins. (B) Diagram of the H3.3 constructs expressed as YFP- or GST-fusion proteins in the recruitment and in vitro binding assays (Figure 3D). The amino acid differences between H3.3 and H3.2/H3.21 are shown in red. The red asterisks in the 4-PTM construct represent K37A, R42A, R49A, and R52A. (C) Localization of H3.3-YFP, expressed in U2OS 2-6-3 cells for 18 (a–d) and 48 h (e–h), in relation to the activated transgene array, marked by Cherry-tTA-ER. Localization of H3.3 N-tail-αN-YFP expressed for 18 (i–l) and 48 h (m–p). Arrows indicate the transgene array, and arrowheads indicate nucleoli. Yellow lines in enlarged merge insets (c, g, k, and o) show the path through which the red and green signals were measured in the intensity profiles (d, h, l, and p). Asterisks mark the start of the measured line. Scale bar, 5 μm, 1 μm (enlarged inset). (D) Percentage of transcriptionally activated cells with enrichment of H3.3-YFP and H3.3 N-tail-αN-YFP at the active transcription site and in nucleoli 18 and 48 h posttransfection. For each time point, 100 cells were counted from three independent transfections. SDs are shown in the form of error bars; *p* values were calculated using the unpaired *t* test.

complex with transcribed S and AS RNA that is distinct from the DNA/chromatin, (Newhart *et al.*, 2012, 2013b). This can also be seen in the signal intensities in the line drawn through the merged image (Figure 1C, enlarged inset in c); the red and green signals do not completely overlap.

By 48 h, H3.3 is incorporated into chromatin in the majority of cells, as determined by the change in its localization pattern; it is distributed evenly throughout the nucleus and excluded from nucleoli (Figure 1C, e–g). Consequently the number of cells with H3.3 enriched in nucleoli decreases by 48 h (Figure 1D). At this later time point, most cells have passed through S phase at least once. Therefore the replication-coupled (RC) and RI H3.3 chromatin assembly machines have likely incorporated the majority of the transiently expressed H3.3-YFP into chromatin by this time. The number of cells with accumulation of H3.3-YFP at the activated array is also reduced by 48 h, suggesting that it is recruited to the transcription site from a nucleosome-free pool.

In contrast to full-length H3.3, H3.3-N-tail-αN is enriched in nucleoli in 100% of cells and recruited to the activated array in ~80% of cells at both time points (Figure 1, C, i–p, and D). This indicates that the H3.3 N-terminus mediates its recruitment to both nucleoli and the transcription site. The incorporation of H3 histones into nucleosomes depends on the interaction of the H4 and H3 histone fold domains (i.e., helixes α1-α2-α3; Luger *et al.*, 1997). Therefore the H3.3-N-tail-αN construct cannot be assembled into nucleosomes and is likely a transition-state mutant that remains in association with upstream regulatory factors.

Screen identifies nucleolar RNA proteins recruited to the activated transgene array

Because nucleolar factors are predicted to regulate DAXX-ATRX–mediated de novo heterochromatin assembly in zygotes (Fulka and Langerova, 2014), we screened YFP-tagged nucleolar proteins for recruitment to the activated array in U2OS cells (Figure 2) with the goal of identifying novel regulators of this pathway. Owing to lower expression, a longer exposure of YFP-NOP56 and NOP58 on the same immunoblot is shown (Figure 2A, boxed region). Using this

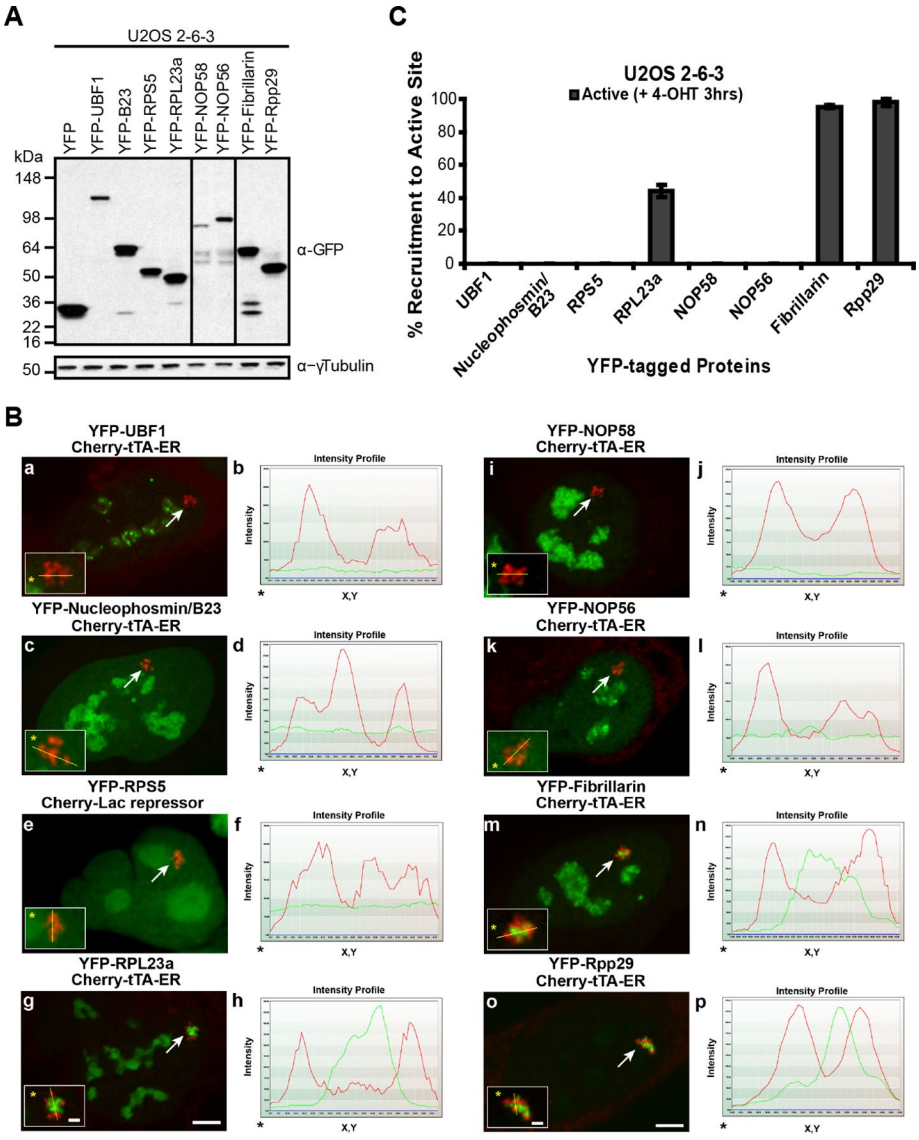

FIGURE 2: Nucleolar proteins are recruited to the activated transgene array. (A) Western blot of the YFP-tagged nucleolar proteins screened for recruitment to the activated transgene array U2OS 2-6-3 cells detected with α-GFP antibody; γ-tubulin is used as a loading control. Owing to the weaker signals of YFP-NOP56 and YFP-NOP58, a longer exposure of the same gel is shown (outlined region). (B) Merged images of the YFP-tagged nucleolar proteins and Cherry-tTA-ER, which marks the activated transgene array (a, c, e, g, i, k, m, and o). Arrows indicate the location of the transgene array. Yellow lines in enlarged insets show the path through which the red and green intensities were measured in the intensity profiles (b, d, f, h, j, l, n, and p). Asterisks mark the start of the measured line. Scale bar, 5 μm, 1 μm (enlarged inset). (C) Percentage of cells with recruitment of the YFP-tagged nucleolar proteins to the activated transgene array. One hundred cells were counted from three independent transfections. SDs are shown in the form of error bars.

approach, we detected recruitment of RPL23a, fibrillarin, and Rpp29 (Figure 2B, g, m, and o, and C). The intensity profiles to the right of the images indicate that, similarly to H3.3, they accumulate in a complex that is distinct from Cherry-tTA-ER, which marks the DNA/chromatin (Figure 2B, h, n, and p). Separate images of the nucleolar proteins and Cherry-tTA-ER are shown in Supplemental Figure S2. Accumulation of Rpp29, fibrillarin, and RPL23a is not seen at the inactive array, marked by Cherry-lac repressor, suggesting that their recruitment is mediated by transcription (Figure 3A).

Fibrillarin is a 2′-O-methyltransferase; as a component of Box C/D small nucleolar ribonucleoproteins (snoRNPs), which also include NOP56, NOP58, and 15.5, it methylates rRNA (Kiss *et al.*, 2006). The lack of NOP58 and NOP56 recruitment (Figure 2B, i and k) suggests that fibrillarin has a snoRNP-independent function at the array. The recruitment of RPL23a supports the hypothesis that ribosomal proteins have noncanonical functions (Bhavsar *et al.*, 2010). Rpp29 is a component of the multisubunit endoribonuclease RNase P, which cleaves the 5′ tRNA leader, and the eukaryotic RNase P variant RNase MRP, which processes mitochondrial RNA and rRNA (Marvin and Engelke, 2009). The recruitment of Rpp29 suggests that other RNase P and RNase MRP subunits may also be recruited.

RPL23a, fibrillarin, and Rpp29 are corecruited with H3.3 to the activated transgene array

To determine the spatial relationship between H3.3 and the nucleolar proteins at the activated array, we coexpressed them (Figure 3B). Rpp29, fibrillarin, and RPL23 colocalize with H3.3-CFP, as confirmed by both the intensity profiles (Figure 3B, d, h, and l) and Pearson's coefficient analysis (Figure 3C), which measures the strength of the linear relationship between two variables. A value of +1 indicates a positive correlation, 0 indicates no correlation, and −1 indicates a negative correlation. YFP-tTA-ER and Cherry-tTA-ER both bind to the TRE repeats in the transgene and were analyzed as a positive control ($r \approx 0.9$; Figure 3C) and Cherry-tTA-ER and H3.3-YFP, which do not colocalize (Figure 1C, a–c), as a negative control ($r = -0.04$). Rpp29, fibrillarin, and RPL23a were all positively correlated with H3.3 ($r \approx 0.9$) but not Cherry-tTA-ER, suggesting that they are components of the H3.3/RNA complex that accumulates at the activated array.

H3.3 forms a biochemical complex with Rpp29, fibrillarin, and RPL23a

To determine whether H3.3 interacts biochemically with the nucleolar proteins, we incubated lysates from cells expressing YFP-tagged Rpp29, fibrillarin, and RPL23a with bacterially expressed glutathione *S*-transferase (GST)–H3.3-N-tail-αN constructs (Figures 1B and 3D). We used both WT H3.3 and a construct containing four point mutations (4-PTMs) in and around the αN helix, which we previously reported reduce both recruitment to the activated array and affinity for double-strand RNA in vitro (Newhart *et al.*, 2013b). Rpp29, fibrillarin, and RPL23a all interact with GST-H3.3 WT but not GST, supporting the hypothesis that associations with nucleolar factors mediate H3.3 recruitment to both nucleoli and the activated array. The interaction between Rpp29 and H3.3 was reduced by the 4-PTMs, indicating that these residues are important for the association. As a positive control, we show that DAXX interacts with WT H3.3 but not the

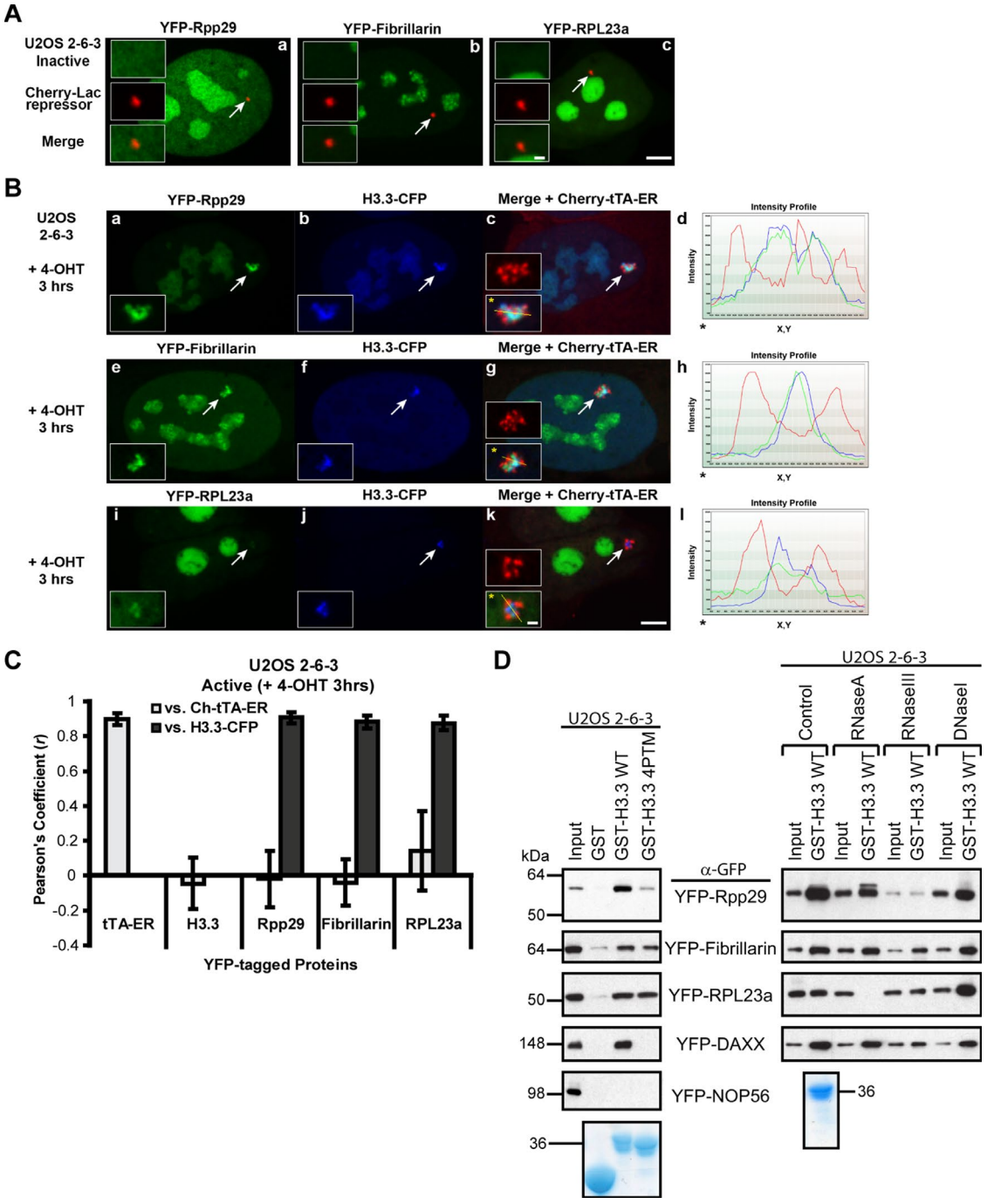

FIGURE 3: Histone H3.3 forms a complex with Rpp29, fibrillarin, and RPL23a. (A) Localization of YFP-Rpp29, YFP-fibrillarin, and YFP-RPL23a in relation to the inactive transgene array in U2OS 2-6-3 cells marked by Cherry-lac repressor (arrows). Scale bar, 5 μm, 1 μm (enlarged inset). (B) Localization of YFP-Rpp29 (a–d), YFP-Fibrillarin (e–h) and YFP-RPL23a (i–l) in relation to H3.3-CFP and the activator, Cherry-tTA-ER, which is shown in the top enlarged insets in c, g, and k. Yellow lines in enlarged merge insets (bottom inset, c, g, and k) show the path through which the red, green, and blue intensities were measured in the intensity profiles (d, h, and l). Asterisks mark the start of the measured line. (C) Pearson's *r* analysis of the overlap between YFP-tagged proteins and Cherry-tTA-ER (white bars) and H3.3-CFP (gray bars) at the activated transgene array. The correlation between Cherry-tTA-ER and YFP-tTA-ER ($n = 10$) was analyzed as a positive control. Cherry-tTA-ER and H3.3-YFP ($n = 11$) were analyzed as a negative control. Rpp29 ($n = 11$), fibrillarin ($n = 10$), and RPL23a ($n = 13$) were compared with both Cherry-tTA-ER and H3.3-CFP. (D) Analyses of interactions between YFP-tagged proteins, detected with α-GFP antibody, and the bacterially expressed GST proteins, GST, GST-H3.3 (N-tail-αN) wild type (WT), and the 4-PTM construct (diagram in Figure 1B), detected by colloidal blue staining. Right, analysis of the effects of RNase A, RNase III, and DNase I treatments on binding.

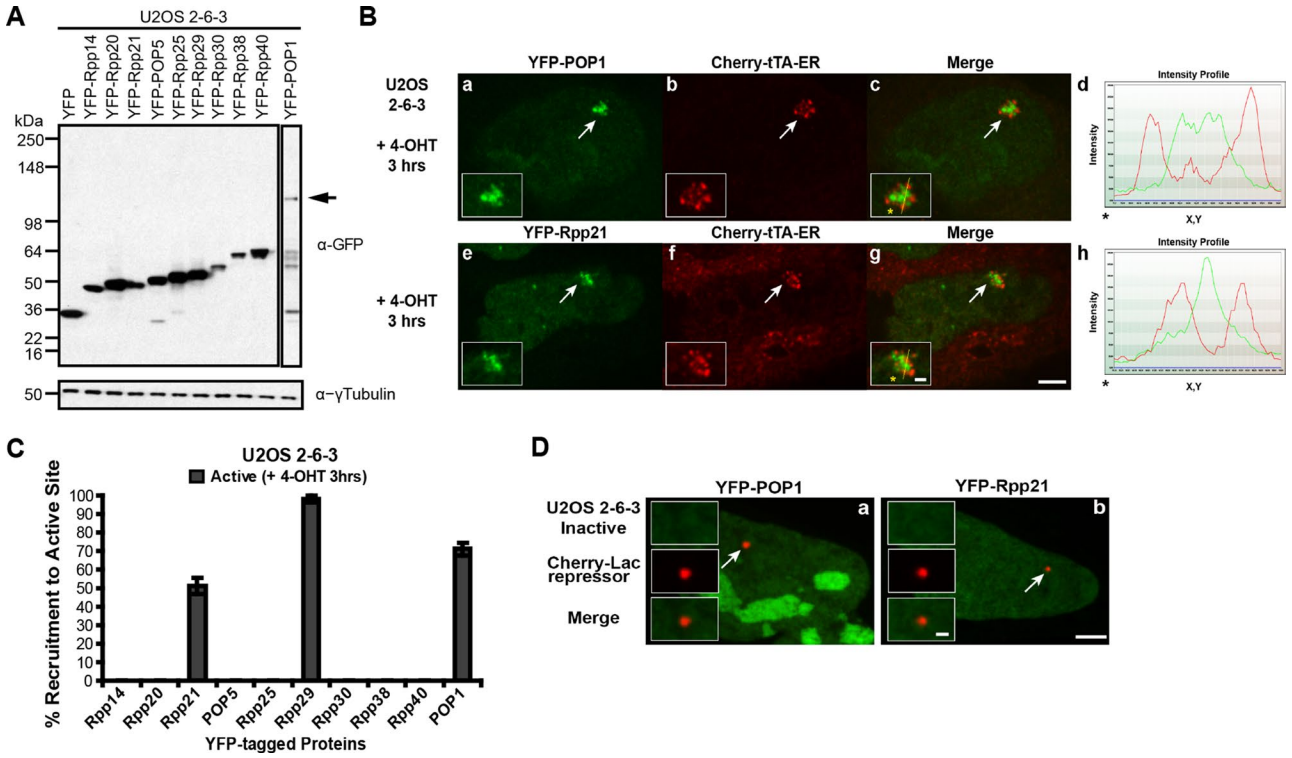

FIGURE 4: The RNase P subunits POP1 and Rpp21 are recruited to the activated transgene array. (A) Western blot of the YFP-tagged RNase P and RNase MRP protein subunits, screened for recruitment to the activated transgene array in U2OS 2-6-3 cells, using α-GFP antibody; γ-tubulin is used as a loading control. Arrow indicates YFP-POP1. Owing to the weak signal of YFP-POP1 on the blot, a longer exposure of the same gel is shown in the outlined region. (B) Localization of YFP-POP1 (a–d) and YFP-Rpp21 (e–h) at the activated transgene array in relation to the activator, Cherry-tTA-ER. Arrows indicate the location of the transgene array. Yellow lines in enlarged merge insets show the path through which the red and green intensities were measured in the intensity profiles (d, h). Asterisks mark the start of the measured line. Scale bar, 5 μm, 1 μm (enlarged inset). (C) Percentage of cells in which the YFP-tagged RNase P/MRP subunits are recruited to the activated transgene array. One hundred cells were counted from three independent transfections. SDs are shown in the form of error bars. (D) Localization of YFP-POP1 and YFP-Rpp21 in relation to the inactive transgene array marked by Cherry-lac repressor.

4-PTM construct (Elsasser *et al.*, 2012) and, as a negative control, that the nonrecruited nucleolar protein NOP56 does not interact with either.

The H3.3–Rpp29 interaction is not nucleic acid dependent

Because Rpp29, fibrillarin, and RPL23a are present in the H3.3/RNA complex at the activated transgene array (Newhart *et al.*, 2013b), we wanted to determine whether nucleic acids are required for their interaction with the GST-H3.3 WT construct. Therefore we pretreated the cell lysates with enzymes to degrade single-stranded RNA (RNase A), double-stranded RNA (RNase III), and DNA (DNase I) before incubation. None of these treatments eliminated the interactions between H3.3 and Rpp29, fibrillarin, or DAXX, indicating that they are not RNA or DNA dependent (Figure 3D). The decrease in YFP-Rpp29 levels in both the RNase III input and pull-down samples is presumably a result of its destabilization in the reaction buffer. Of interest, RNase A eliminates the H3.3–RPL23a interaction, indicating dependence on single-stranded RNA.

The RNase P protein subunits POP1 and Rpp21 are recruited to the activated transgene array

Because H3.3 accumulates with S and AS RNA transcribed from the transgene array (Newhart *et al.*, 2013b) and RNase P degrades AS RNA in yeast (Marvin *et al.*, 2011), we focused on investigating the function of Rpp29 in transcription and H3.3 chromatin assembly. In bacteria, RNase P is composed of a catalytic RNA and a single protein subunit that structurally resembles eukaryotic POP5 (Wilson *et al.*, 2006). In addition to a catalytic RNA, archaeal RNase P includes four proteins homologous to eukaryotic Rpp21, POP5, Rpp29, and Rpp30. Eukaryotic RNase P contains ~10 proteins, most of which are shared with RNase MRP (Marvin and Engelke, 2009). To determine whether any of the other RNase P and RNase MRP proteins are recruited to the activated array, we evaluated YFP-tagged versions (Figure 4A). Only POP1 and Rpp21 accumulated and, similarly to Rpp29, did not colocalize with Cherry-tTA-ER, which suggests that they also reside in the H3.3/RNA complex (Figure 4, B and C, and Supplemental Figure S3). POP1 and Rpp21 were not detected at the inactive array, marked by Cherry-lac repressor (Figure 4D), indicating that their accumulation is also linked to transcription.

The RNase P and MRP catalytic RNAs do not accumulate at the activated transgene array

To investigate whether the RNase P and/or MRP catalytic RNAs are recruited to the activated array, we used RNA fluorescence in situ hybridization (RNA FISH) to evaluate their localization. It was previously shown that RPPH1, the human RNase P catalytic RNA, localizes in a diffuse pattern throughout the nucleus and that the RNase MRP RNA, RMRP, is enriched in nucleoli (Jacobson *et al.*, 1997).

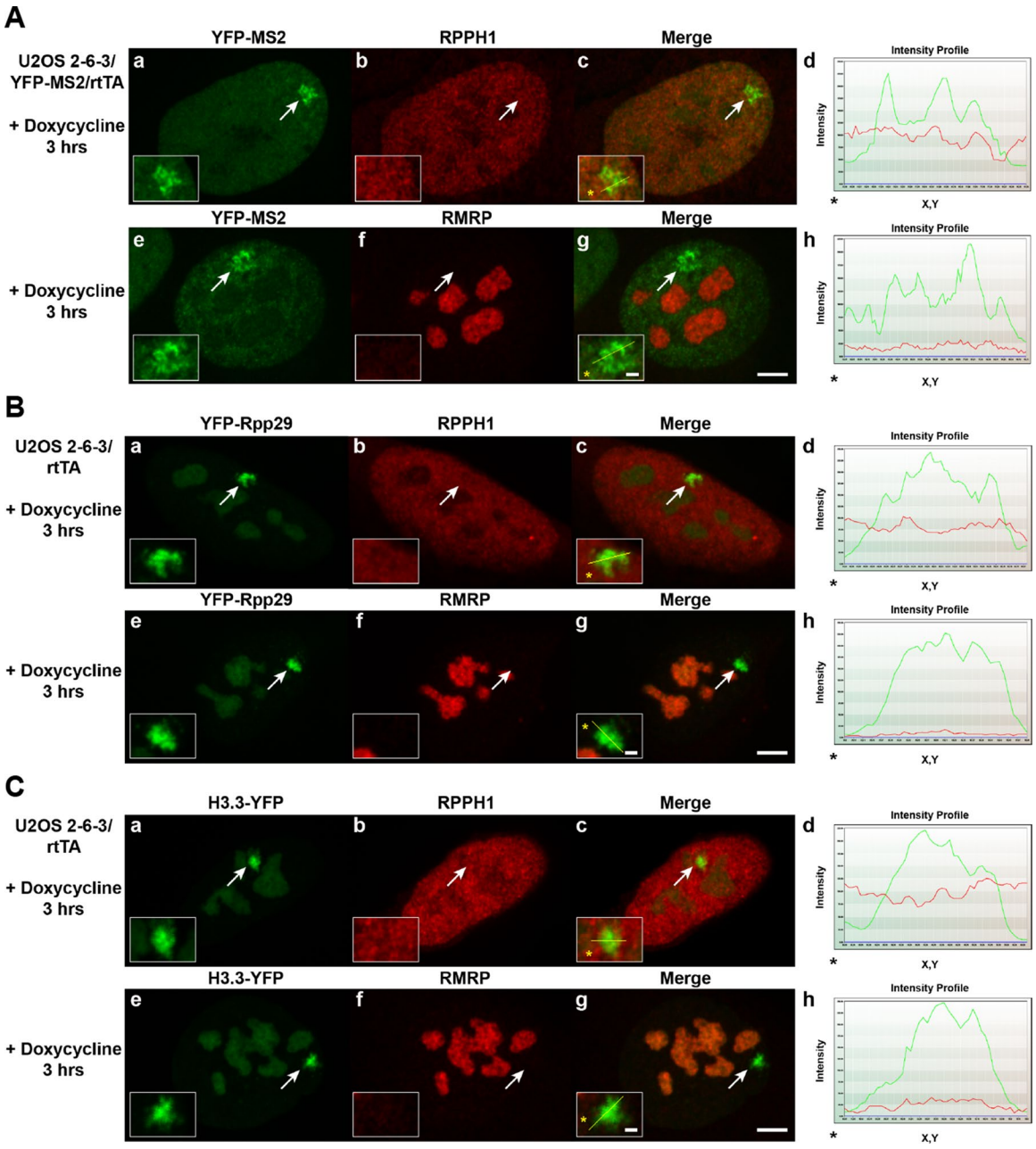

FIGURE 5: The RNase P and RNase MRP catalytic RNAs are not recruited to the activated transgene array. (A) Strand-specific RNA FISH probes were used to visualize the RNase P (RPPH1; a–d) and RNase MRP (RMRP; e–h) catalytic RNAs at the activated transgene array in U2OS 2-6-3 stably expressing YFP-MS2 and rtTA. YFP-MS2 was used to mark the active site (arrows). Yellow lines in enlarged merge insets show the path through which the red and green intensities were measured in the intensity profiles (d, h). Asterisks mark the start of the measured line. Scale bar, 5 μm, 1 μm (enlarged inset). (B) Localization of the RNase P (RPPH1; a–d) and RNase MRP (RMRP; e–h) catalytic RNAs at the activated transgene array in U2OS 2-6-3 cells expressing YFP-Rpp29. Transcription was induced with the activator rtTA (+) Dox. (C) Localization of the RNase P (RPPH1; a–d) and RNase MRP (RMRP; e–h) catalytic RNAs at the activated transgene array in U2OS 2-6-3 cells expressing H3.3-YFP.

Although we detected RPPH1 and RMRP in their previously reported patterns, neither accumulated at the activated array, marked by YFP-MS2 (Figure 5A). To determine whether we could detect accumulation when either H3.3 or Rpp29, which interacts directly with RPPH1 and RMRP (Marvin and Engelke, 2009), is enriched at the site, we performed RNA FISH in YFP-Rpp29– and H3.3-YFP-expressing cells. The fact that neither RPPH1 nor RMRP accumulated under these conditions (Figure 5, B and C) suggests either that they do not function at the array or that their functions are dysregulated in U2OS cells.

Rpp29 recruitment dynamics suggests that it suppresses transcription

The recruitment of Rpp29 to the activated transgene array suggested that it might regulate transcription. To investigate the effect of Rpp29 on transcription, we imaged the transgene array in single

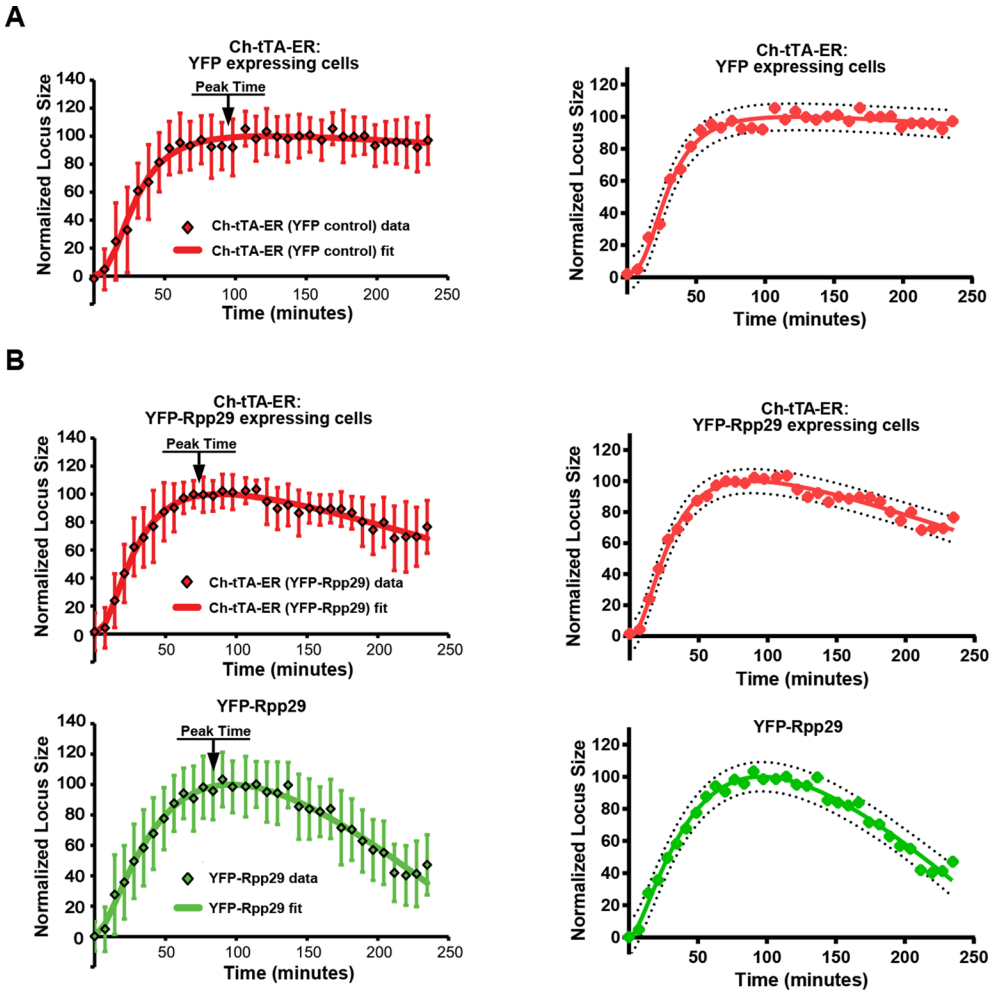

C

Peak (time accumulation reaches 99% of maximum) and fitted slope (m) of the linear decrease.

	PHASE 1: Peak (min)	PHASE 2: Slope
Ch-tTA-ER (YFP control)	95	-0.07
Ch-tTA-ER (YFP-Rpp29)	75	-0.31
YFP-Rpp29	84	-0.86

D

Fitting Parameters. Errors represent 95% confidence intervals on fit.

	A1	A2	x0	p	m (slope)
Ch-tTA-ER (YFP control)	-0.1 ± 6.6	113 ± 13	29 ± 3	2.3 ± 0.6	-0.07 ± 0.06
Ch-tTA-ER (YFP-Rpp29)	0 ± 6.6	144 ± 17	30 ± 4	1.9 ± 0.4	-0.31 ± 0.07
YFP-Rpp29	0 ± 7.8	216 ± 84	57 ± 18	1.4 ± 0.3	-0.86 ± 0.23

FIGURE 6: Single-cell analysis of Rpp29 recruitment dynamics suggests that it suppresses transcription at the activated transgene array. (A) Quantification of the changes in the area of the transgene array in U2OS 2-6-3 cells, as detected by Cherry-tTA-ER (red) intensity, during transcriptional activation in YFP-expressing control cells. 4-OHT was added to the medium immediately after the second image in the time series was acquired. Images were collected every 7.5 min for 4 h. Measured areas were normalized to the high and low plateau values and fitted to a model (solid lines). Peak values are indicated in the graphs. Error bars represent SD. Data and fit are shown with 95% prediction bands for the fitted curve (dotted lines, right). (B) Quantification of the areas occupied by Cherry-tTA-ER (red) and YFP-Rpp29 (green) at the transgene array during the course of transcriptional activation. Cherry-tTA-ER values from individual control and YFP-Rpp29–expressing cells are depicted in Supplemental Figure S4. (C) Table of phase 1 and phase 2 peaks and phase 2 slope values. (D) Table of fitting parameters. No overlap is seen in the confidence intervals on the fits of the slopes after peak times.

cells over the course of ~4 h of activation (Figure 6, Supplemental Movie S1, and Supplemental Figure S4). For these analyses, the pixel intensities of Cherry-tTA-ER and YFP-Rpp29 at the transgene array were thresholded and measured. We previously reported that the area of the array, marked by Cherry-tTA-ER, increases after induction due to chromatin decondensation driven by RNA pol II activity (Rafalska-Metcalf *et al.*, 2010). Therefore this analysis can be used to gain insight into transcriptional dynamics.

Using this approach, we determined that during activation, the initial increase in the area of the transgene array, marked by Cherry-tTA-ER, is approximately exponential in both YFP- and YFP-Rpp29–expressing cells (Figure 6, A and B). Over time, growth slows, eventually stops, and decreases, which suggests the transcription decreases after the peak. By fitting the curve to a function that combines a growth model dominating in phase 1 (before the peak) and a linear model dominating in phase 2 (after the peak), we were able to measure and compare temporal profiles and parameters between YFP- and YFP-Rpp29–expressing cells (Figure 6, C and D). Cherry-tTA-ER peaked earlier (75 vs. 95 min) and decreased more rapidly after its peak in cells expressing YFP-Rpp29 than in those expressing

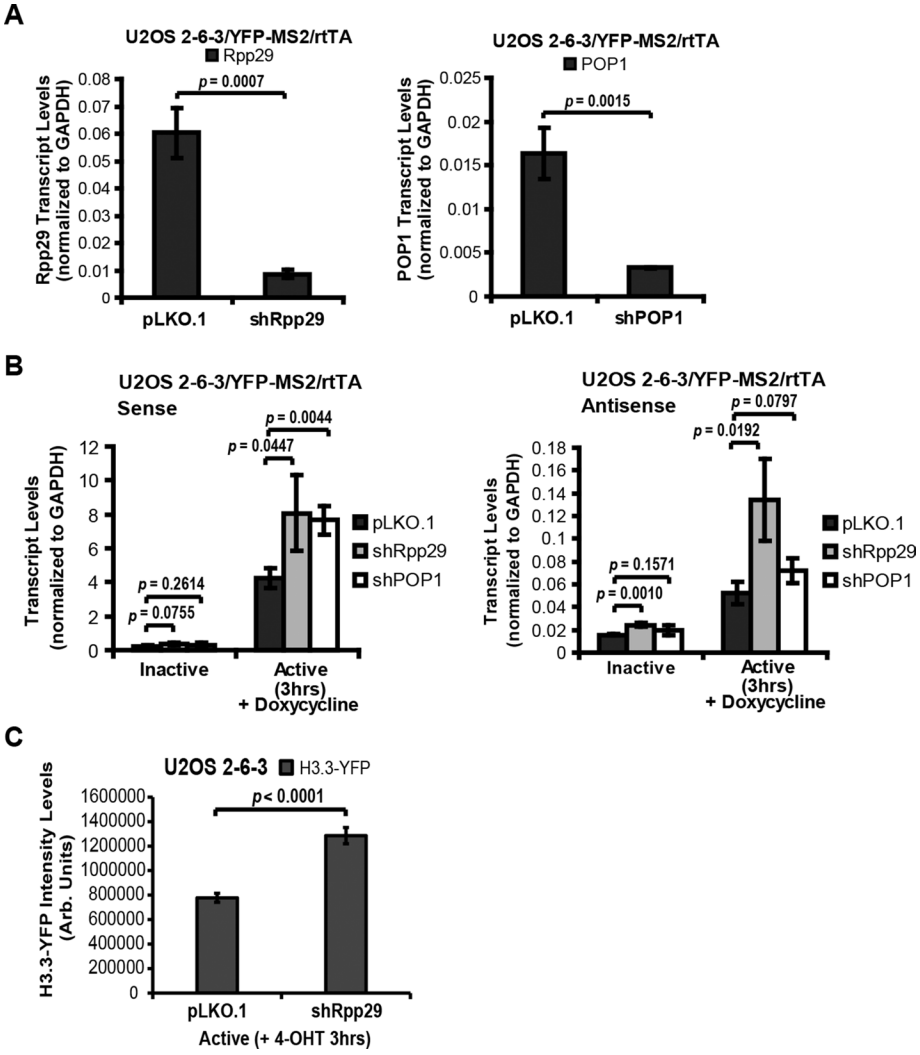

FIGURE 7: Rpp29 and POP1 repress transcription from the transgene array. (A) qRT-PCR analysis of Rpp29 and POP1 mRNA levels in U2OS 2-6-3 cells stably expressing YFP-MS2 and rtTA cells after shRNA knockdown. SDs are shown in the form of error bars; *p* values were calculated using an unpaired *t* test ($n = 3$). (B) Strand-specific qRT-PCR analysis of total RNA isolated 0 and 3 h after activation in U2OS 263 cells stably expressing YFP-MS2 and rtTA after shRNA knockdown. A primer pair in rabbit β-globin exon 3 was used for PCR. (C) Measurement of the intensity of H3.3-YFP recruited to the activated transgene array in U2OS 2-6-3 cells after control (pLKO.1; $n = 30$) and Rpp29 ($n = 31$) knockdown.

YFP (slope –0.31 vs. –0.07; $p < 0.0001$), suggesting that Rpp29 accelerates chromatin recondensation. The finding that YFP-Rpp29 both accumulated and peaked later than Cherry-tTA-ER (84 vs. 75 min; Figure 6C) supports the conclusion that Rpp29 recruitment depends on transcription. The rapid decrease in YFP-Rpp29 levels at the array after their peak (phase 2 slope, –0.86) also suggests that Rpp29 functions in the processing/degradation of an RNA substrate that, as it is consumed, results in reduced association of Rpp29 with the site. Taken together, these results suggest that Rpp29 represses transcription from the transgene array.

Rpp29 and POP1 repress transgene RNA levels in U2OS cells

To test the hypothesis that Rpp29 represses transcription, we knocked down Rpp29, as well as POP1, in the U2OS cell line and measured S and AS RNA levels. Figure 7A shows the depletion of Rpp29 and POP1 mRNA in short hairpin RNA (shRNA)–expressing cells. Knockdown of Rpp29 significantly increased levels of both S (activated cells) and AS RNA (inactive and activated cells), whereas POP1 knockdown increased S RNA levels (activated cells; Figure 7B). This result supports the hypothesis that Rpp29, as well as POP1, represses transcription from the transgene array.

Rpp29 represses H3.3 recruitment to the activated transgene array in U2OS cells

The finding that H3.3 accumulates with transcribed S and AS RNA at the activated array suggested that H3.3 is recruited to its incorporation sites by a transcriptional signal (Newhart *et al.*, 2013b). To determine whether Rpp29 regulates H3.3 recruitment to the activated array in the U2OS cell line, we evaluated the effect of knockdown on H3.3-YFP accumulation, using quantitative image analysis (Figure 7C). The intensity of the H3.3-YFP signal increased significantly after Rpp29 knockdown, which supports the model in which Rpp29 represses a transcriptional signal that recruits H3.3 to its incorporation sites.

Rpp29 represses the incorporation of H3.3 into the transgene array chromatin

To determine whether Rpp29 regulates H3.3 nucleosome deposition, we knocked Rpp29 down in the HeLa cell line stably expressing H3.3-YFP (Figure 8A) and evaluated H3.3 incorporation into the inactive transgene array using chromatin immunoprecipitation (ChIP; Figure 8B is a diagram of the procedure). We previously reported that, in the HeLa cell line, H3.3 is significantly enriched in the inactive transgene array (Figure 8D is a diagram of the primer pairs) compared with the RC variant, H3.2 (Newhart *et al.*, 2012). Here we show that Rpp29 knockdown significantly increases H3.3 incorporation into the array (Figure 8E, brown bars). Taken together, these results suggest that Rpp29 represses H3.3 chromatin assembly by downregulating a transcriptional recruitment signal.

We also analyzed the effects of ATRX knockdown (Figure 8C) on H3.3 incorporation into the transgene array because of its reported requirement for H3.3 deposition into repetitive regions, including telomeres and pericentromeres (Drane *et al.*, 2010; Goldberg *et al.*, 2010; Lewis *et al.*, 2010) and reports that ATRX regulates RNA-mediated chromatin events (Sarma *et al.*, 2014; Flynn *et al.*, 2015). Surprisingly, ATRX knockdown did not detectably affect H3.3 incorporation into the HeLa cell transgene array (Figure 8E, orange bars). Loss of ATRX is a hallmark of cells, including U2OS, that use the alternative lengthening of telomere (ALT) pathway to maintain telomere length (Heaphy *et al.*, 2011; Bower *et al.*, 2012; Lovejoy *et al.*, 2012). However, ATRX knockdown is insufficient to induce ALT (Clynes *et al.*, 2014; Episkopou *et al.*, 2014; O'Sullivan *et al.*, 2014). Taken together, these results suggest that additional mechanisms must be dysregulated in

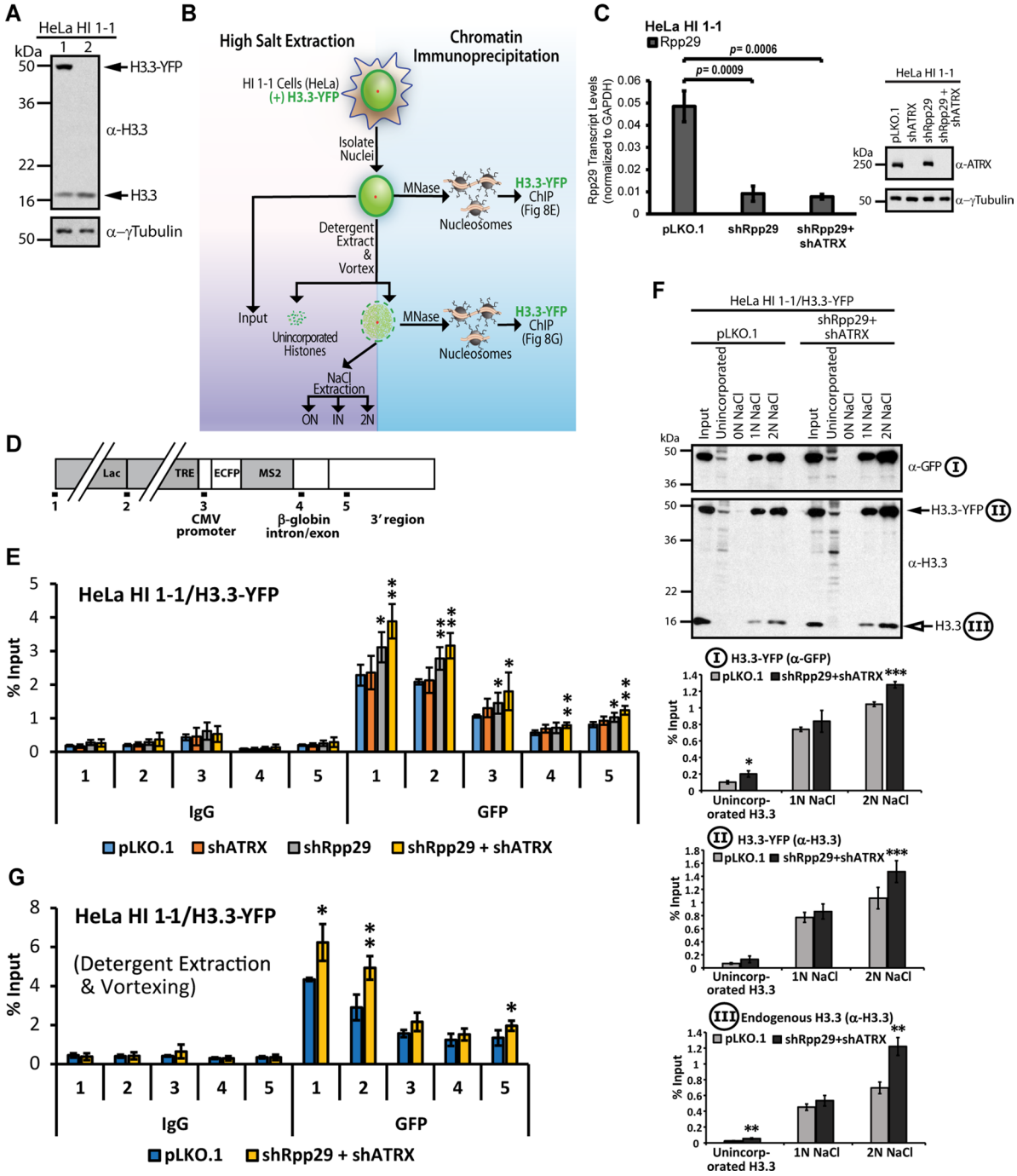

FIGURE 8: Rpp29 represses histone H3.3 chromatin assembly. (A) Western blot shows levels of endogenous H3.3 and H3.3-YFP in the HeLa HI 1-1/H3.3-YFP (lane 1) and HeLa HI 1-1 (lane 2) cell lines. (B) Diagram of the steps undertaken in the high-salt extraction and chromatin immunoprecipitation protocols. (C) qRT-PCR and Western blot analysis of Rpp29 mRNA and ATRX protein levels, respectively, in HeLa HI 1-1 cells after shRNA knockdown. For qRT-PCR, results are the average of three independent experiments. SDs are shown in the form of error bars; *p* values were calculated using unpaired *t* test. (D) The transgene diagram shows the location of the primer pairs used for qPCR analysis of the ChIP results in HeLa HI 1-1/H3.3-YFP cells. (E) ChIP analysis of H3.3-YFP incorporation into the transgene array after knockdowns in HeLa HI 1-1/H3.3-YFP cells. Results are the average of at least three independent experiments, and *p* values were calculated by comparing pLKO.1 (blue bar) to the shRNA data sets using unpaired *t* test: $*p \leq 0.05$ and $**p \leq 0.01$. (F) Representative Western blot of high-salt extraction assay showing H3.3-YFP and H3.3 levels detected using anti-GFP and anti-H3.3 antibodies. Graphs show measurements of (I) H3.3-YFP with anti-GFP antibody, (II) H3.3-YFP with anti-H3.3 antibody, and (III) H3.3 with anti-H3.3 antibody. Results are the average of at least three independent experiments, and *p* values were calculated using unpaired *t* test: $*p \leq 0.05$, $**p \leq 0.01$, and $***p \leq 0.001$. (G) ChIP analysis of H3.3-YFP incorporation into the transgene array in HeLa HI 1-1/H3.3-YFP cells after first detergent extracting and vortexing isolated nuclei.

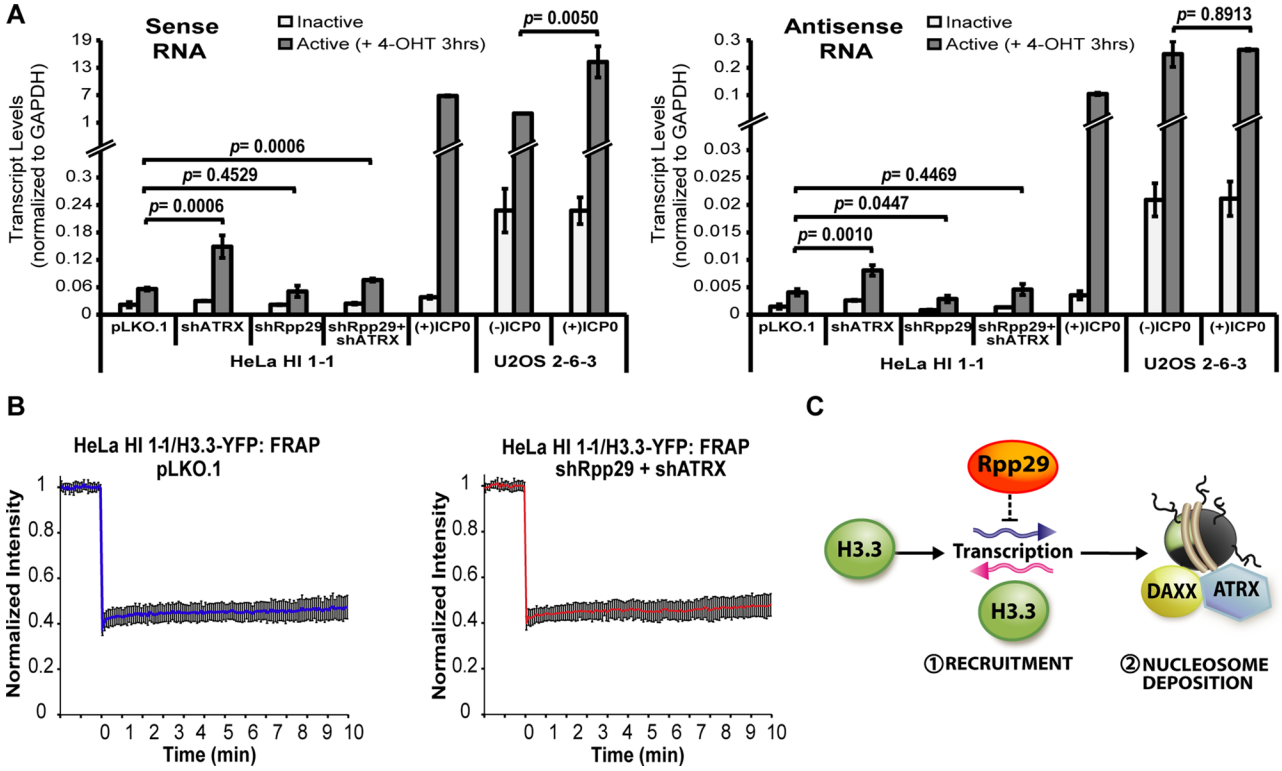

FIGURE 9: Rpp29 is not required for maintenance of transcriptional silencing. (A) Strand-specific qRT-PCR analysis of sense and antisense transgene RNA levels in inactive and activated HeLa HI 1-1 and U2OS 2-6-3 cells after shRNA knockdown of Rpp29 and ATRX and ICP0 expression. The pLKO.1 vector was used as a control. A primer pair in rabbit β-globin exon 3 was used for PCR. Results are the average of at least three independent experiments. SDs are shown in the form of error bars; *p* values were calculated using unpaired *t* test. (B) Graphs of the average FRAP of H3.3-YFP in HeLa HI 1-1/H3.3-YFP cells over the course of 10 min of imaging. ShRNA constructs were expressed for 72 h before photobleaching: control pLKO.1 ($n = 14$) and Rpp29+ATRX double knockdown ($n = 14$). (C) Model of Rpp29 function in histone H3.3 chromatin assembly at a DAXX-ATRX–regulated site, showing two steps: 1) H3.3 recruitment through a transcriptional signal that Rpp29 functions to down-regulate, and 2) nucleosomal deposition of H3.3 by DAXX and ATRX.

order for ALT to be activated and H3.3 incorporation into the transgene array to be disrupted.

Of interest, Rpp29+ATRX double knockdown increased H3.3 incorporation into the HeLa cell array slightly more than knockdown of Rpp29 alone, which suggests that they functionally interact. Although many studies indicate that ATRX is required for H3.3 chromatin incorporation (Drane *et al.*, 2010; Goldberg *et al.*, 2010; Wong *et al.*, 2010), increased H3.3 deposition has also been detected after ATRX knockout in mouse forebrain (Levy *et al.*, 2015). These results suggest that the mechanistic basis of ATRX function has yet to be fully elucidated.

Rpp29 represses genome-wide H3.3 chromatin incorporation

To determine the effect of Rpp29+ATRX double knockdown on genome-wide H3.3 chromatin incorporation, we used a high-salt extraction assay (Figure 8, B and F). Histones, especially H3 and H4, are tightly associated with nucleosomes but can be solubilized by 2 M NaCl (Shechter *et al.*, 2007). Compared to the control, significantly higher levels of H3.3-YFP and endogenous H3.3 were extracted from Rpp29+ATRX–knockdown cells (Figure 8F) suggesting that their depletion increases H3.3 chromatin incorporation genome wide. Due to the significant increase in unincorporated H3.3 in Rpp29+ATRX–knockdown cells (Figure 8F), we also performed ChIP at the transgene array after first detergent extracting and vortexing isolated nuclei (Figure 8B), which confirmed that unincorporated H3.3 does not contribute to the increase in array deposition (Figure 8, E and G).

Rpp29 is not required to maintain transcriptional silencing

To decipher the link between H3.3 chromatin incorporation and transcriptional silencing, we knocked Rpp29 down in the HeLa cell line and measured S and AS transgene RNA levels 3 h after activation (Figure 9A). Compared to control cells (pLKO.1), Rpp29 knockdown did not significantly increase S and AS RNA expression, which suggests that Rpp29 is not required to maintain silencing. In fact, the increase in H3.3 deposition that accompanies Rpp29 knockdown (Figure 8E) may suppress array activation, because H3.3 chromatin assembly is required for the establishment of heterochromatic histone PTMs, including H3K27me3 at HIRA-regulated bivalent genes (Banaszynski *et al.*, 2013) and H3K9me3 at DAXX-ATRX–regulated sites (Elsasser *et al.*, 2015; He *et al.*, 2015; Jang *et al.*, 2015; Udugama *et al.*, 2015; Voon *et al.*, 2015).

In contrast to Rpp29, ATRX knockdown significantly increased S and AS RNA levels (Figure 9A), which suggests that ATRX contributes to maintenance of silencing. Although we did not detect a decrease in H3.3 incorporation after ATRX knockdown (Figure 8E), it is possible that even a small reduction promotes transcription. Of interest, S and AS RNA levels increased less after Rpp29+ATRX knockdown than after knockdown of ATRX alone, suggesting that

codepletion with Rpp29 counteracts the positive effects of ATRX reduction.

To provide a reference point for S and AS RNA expression from derepressed arrays, we included analyses of U2OS and ICP0-expressing HeLa cells (Figure 9A). ICP0 is a herpes simplex 1 E3 ubiquitin ligase required to reverse latency, which we previously showed derepresses the HeLa cell array (Newhart *et al.*, 2012). Compared to HeLa cells expressing shATRX, S and AS RNA levels are dramatically higher in U2OS and ICP0-expressing HeLa cells, indicating that ATRX knockdown is insufficient to derepress the array. ICP0 also enhances transcription of S RNA from the U2OS cell array, suggesting that its expression is constrained by factors that ICP0 eliminates.

Rpp29+ATRX knockdown does not affect H3.3 nucleosome stability

To investigate the effect of Rpp29+ATRX knockdown on H3.3 nucleosome stability, we used fluorescence recovery after photobleaching (FRAP) in HeLa cells stably expressing H3.3-YFP. Previous reports indicate that H3 histones are stably incorporated into nucleosomes (Kimura and Cook, 2001; Meshorer *et al.*, 2006). To examine the long-term recovery kinetics of H3.3, we imaged cells every 10 s for 10 min after bleaching (Figure 9B). Minimal recovery of H3.3-YFP was detected in both control and shRpp29+shATRX cells, indicating that their knockdown does not affect nucleosome stability.

Rpp29 down-regulates H3.3 chromatin assembly by repressing a transcriptional signal that recruits H3.3 to its incorporation sites

On the basis of our identification of Rpp29 as a factor that interacts with H3.3 upstream of nucleosome deposition and the finding that Rpp29 knockdown increases H3.3 recruitment to and incorporation into chromatin, we propose a two-step model for H3.3 nucleosome deposition (Figure 9C). First, H3.3 is recruited to its incorporation sites by a transcriptional signal that Rpp29 functions to repress. In the second step, chromatin assembly factors, such as DAXX and ATRX, regulate H3.3 incorporation into nucleosomes. Because H3.3 deposition is linked to the establishment of histone PTMs (Banaszynski *et al.*, 2013; Elsasser *et al.*, 2015; He *et al.*, 2015; Jang *et al.*, 2015; Udugama *et al.*, 2015; Voon *et al.*, 2015), the finding that Rpp29 regulates H3.3 chromatin assembly by repressing deposition could have important implications for understanding how transcription states are established and maintained.

DISCUSSION

Histone H3.3 is an important regulator of transcription-state change and epigenetic inheritance, but apart from the chaperoning complexes that regulate nucleosome incorporation, few other pathway components have been identified. In this study, we show that the newly expressed H3.3, which is enriched in nucleoli (Delbarre *et al.*, 2012), is recruited to these nuclear structures through N-terminal sequence elements. Recently it was reported that nucleolar factors of unknown identity are required for DAXX-ATRX–mediated de novo assembly of pericentric DNA into heterochromatin in zygotes (Fulka and Langerova, 2014). This suggests that the nucleolar association of H3.3 is functionally significant.

We previously reported that a transgene array, which can be directly visualized in single cells, is regulated by the DAXX-ATRX-H3.3 pathway (Newhart *et al.*, 2012). When integrated into ATRX-null U2OS cells, the array can be robustly activated, and H3.3 accumulates at the site in a complex with transcribed S and AS RNA that is distinct from the DNA/chromatin (Newhart *et al.*, 2013b). This suggested that transcriptional mechanisms regulate the recruitment of H3.3 to its deposition sites. Here we extend this analysis to show that the nucleolar RNA proteins Rpp29, fibrillarin, and RPL23a are also components of this H3.3/RNA complex. Rpp29 knockdown increases both the accumulation of H3.3 at the activated array and its incorporation into chromatin, which supports the model that Rpp29 represses H3.3 chromatin assembly by down-regulating a transcriptional recruitment signal (Figure 9C).

Rpp29 is a component of the multisubunit endoribonucleases RNase P and RNase MRP, for which noncoding RNAs function as the catalytic subunits. The colocalization of Rpp29 with H3.3 at the activated array suggested that other subunits of these enzymes would also be recruited. Indeed, POP1 and Rpp21 are similarly recruited, suggesting that H3.3 chromatin assembly is regulated by a variant of RNase P. Because Rpp29 and Rpp21 form an RNA-independent heterodimer in Archaea (Xu *et al.*, 2012), their corecruitment with H3.3 suggests that this ancient interaction is conserved in the predicted variant.

Surprisingly, we did not detect either the RNase P or the RNase MRP catalytic RNA (i.e., RPPH1 and RMRP) at the activated array in U2OS cells, making it possible that neither is a component of this enzyme subcomplex or that RPPH1 or RMRP recruitment to the array is dysregulated in U2OS cells. Alternatively, this variant complex could contain a novel catalytic RNA. We favor the hypothesis that RNA is a component of this variant because in canonical RNase P, Rpp29, POP1, and Rpp21 all interact with RPPH1 (Reiner *et al.*, 2011; Khanova *et al.*, 2012), which suggests that RNA scaffolds enzyme assembly. We do not know the mechanism by which Rpp29 and POP1 repress transcription from the U2OS cell transgene array or why Rpp29, but not POP1, knockdown significantly increases AS RNA levels. If both Rpp29 and POP1 are components of an enzyme complex with activity toward AS RNA, it is possible that its function is more sensitive to Rpp29 depletion.

In contrast to U2OS cells, high levels of S and AS RNA are not expressed from the activated HeLa cell transgene array, consistent with it being transcriptionally silenced (Newhart *et al.*, 2012). Because Rpp29 depletion does not result in a detectable increase in HeLa cell transgene S and AS RNA expression, it suggests that Rpp29 is not required to maintain silencing. However, the ability to analyze the effects of Rpp29 on transcription from the derepressed array in the U2OS cell array allowed us to formulate the hypothesis that Rpp29 regulates H3.3 chromatin assembly by repressing a transcriptional recruitment signal. It is possible that Rpp29 is required to establish silencing at DAXX-ATRX–regulated sites, after which mechanisms, including histone PTMs, function to maintain it through cell division. Of interest, RNase P was recently linked to transcriptional silencing by the finding that Rpp30 is required to repress transposable elements and establish H3K9me3 marks in germ cells (Molla-Herman *et al.*, 2015). In the future, it will be important to determine whether Rpp29 is one of the nucleolar proteins required for the de novo assembly of pericentric heterochromatin in zygotes (Fulka and Langerova, 2014), as well as whether it regulates H3.3 deposition at HIRA-regulated sites.

Copy-number variations in Rpp29 have been detected in breast and ovarian cancer (Wrzeszczynski *et al.*, 2011; Natrajan *et al.*, 2012). In addition, Rpp29, located at 19q12, is in a region commonly codeleted with chromosome 1p in oligodendrogliomas and astrocytomas (Reuss *et al.*, 2014). At this time, it is unknown how Rpp29 copy-number changes contribute to carcinogenesis. Our demonstration that Rpp29 down-regulates H3.3 chromatin incorporation suggests that they could alter gene expression programs by changing the

kinetics of H3.3 chromatin assembly, which is required for deposition of heterochromatic histone PTMs, including H3K27me3 at HIRA-regulated genes (Banaszynski *et al.*, 2013) and H3K9me3 at DAXX-ATRX–regulated sites (Elsasser *et al.*, 2015; He *et al.*, 2015; Jang *et al.*, 2015; Udugama *et al.*, 2015; Voon *et al.*, 2015).

In this study, we concentrated on investigating the function of Rpp29 in DAXX-ATRX–mediated H3.3 chromatin assembly. However, the association of RPL23a and fibrillarin with H3.3 at the activated transgene array suggests that they may also be components of this pathway. Of interest, noncanonical functions for RPL23a and fibrillarin have been reported. Fibrillarin and RPL23a are both enriched in mitotic chromatin (Hayashihara *et al.*, 2010). RPL23a was a top hit in an shRNA screen for factors required for $Hras^{G12V}$-dependent oncogenic growth (Beronja *et al.*, 2013). The yeast fibrillarin orthologue Nop1 methylates histone H2A in ribosomal DNA, and its disruption dysregulates rDNA transcription (Tessarz *et al.*, 2013). Future analyses of the effect of RPL23a and fibrillarin on H3.3 chromatin assembly will expand our understanding of H3.3 function in genome regulation.

A better understanding of H3.3 chromatin assembly could also provide insight into how the gain-of-function point mutations, concentrated in the H3.3 N-terminal tail, drive pediatric brain and skeletal cancers (Lindroth and Plass, 2013). In pediatric glioma, lysine 27 is converted to methionine (K27M), which inhibits the H3 K27 trimethyltransferase EZH2, resulting in a global decrease in H3K27me3 (Bender *et al.*, 2013; Chan *et al.*, 2013; Lewis *et al.*, 2013; Venneti *et al.*, 2013). However, when and where H3.3(K27M) interacts with EZH2 are unknown. Glycine 34 is also mutated to either arginine or valine in pediatric glioma and to tryptophan or leucine in giant cell tumor of the bone; their mechanisms of pathogenesis are unknown. The selective association of the H3.3 point mutations with pediatric tumors suggests that they dysregulate normal development. It will be important to determine whether RNA factors are required for the oncohistone H3.3s to drive tumorigenesis. Therefore an expanded understanding of how transcription and RNA mechanisms regulate H3.3 chromatin assembly could provide new insight into cancer etiology.

MATERIALS AND METHODS

Plasmids

Cherry-lac repressor, Cherry-tTA-ER, H3.3-CFP, H3.3-YFP, H3.3-N-tail-αN-YFP, GST-H3.3-N-tail-αN wild type, GST-H3.3-N-tail-αN 4-PTM, and pLU-YFP-ICP0 were previously described (Janicki *et al.*, 2004; Rafalska-Metcalf *et al.*, 2010; Newhart *et al.*, 2012, 2013a,b). GFP-UBF1-C1, GFP-nucleophosmin/B23-C1, GFP-RPS5-C1, GFP-RPL23a-C1, and GFP-fibrillarin-C1 (gifts of Sui Huang, Northwestern University, Chicago, IL; Chen and Huang, 2001) were converted into YFP-C1 constructs by either replacing GFP with YFP or recloning the insert. YFP-NOP56-C3 and YFP-NOP58-C1 were constructed by PCRing cloning the respective cDNAs (*Xho*I/*Eco*RI and *Xho*I/*Bam*HI). GFP-Rpp14-C1, GFP-Rpp20-C1, GFP-Rpp21-C1, GFP-Pop5-C1, GFP-Rpp29-C1, GFP-Rpp30, GFP-Rpp38-C1, and GFP-Pop1-C1 (gifts of Sidney Altman, Yale University, New Haven, CT; Jarrous *et al.*, 1999, 2001) were converted into YFP-C1 constructs by either replacing GFP with YFP or recloning the insert. YFP-Rpp40-C1 was made by PCR cloning the cDNA (LIFESEQ5687201; Open Biosystems, GE Dharmacon, Huntsville, AL) as an *Xho*I/*Bam*HI fragment.

Cell culture, transfections, and imaging

The U2OS cell lines 2-6-3 and 2-6-3/YFP-MS2/rtTA were previously described (Janicki *et al.*, 2004; Rafalska-Metcalf *et al.*, 2010; Newhart *et al.*, 2012). The HeLa cell lines HI 1-1 and HI 1-1/H3.3-YFP were previously described (Newhart *et al.*, 2012). The cell line 2-6-3/rtTA, used for RNA FISH, was developed as previously described (Rafalska-Metcalf and Janicki, 2013). Transcriptional activation is induced in the 2-6-3/YFP-MS2/rtTA cells by Dox (1 μg/ml) and in 2-6-3 cells expressing tTA-ER activator with 4-OHT (1 μM). Transient transfections were performed using FuGENE (Promega, Madison, WI) as previously described (Newhart *et al.*, 2012).

Imaging

Confocal imaging and time-course imaging were done as previously described (Rafalska-Metcalf *et al.*, 2010; Newhart *et al.*, 2013b). Pearson's *r* was calculated using SimplePCI software (Hamamatsu, Middlesex, NJ) by manually selecting the transgene array site with the region of interest (ROI) function. Intensity profiles for merged pictures were also generated using SimplePCI software.

Image segmentation, tracking, and analysis

The program used to track the changes in factor accumulation at the transgene array (locus) over time segments the locus in each image frame and tracks frame-to-frame segmentation results. To minimize the effects of photobleaching on the analysis, the size of the accumulations rather than their intensity was measured, as it does not require absolute measurements of fluorescence intensity but instead a single decision of relative signal intensity of pixels in the ROI compared with background levels. Delineation of the locus from background begins using a preprocessing detection program previously described (Michel *et al.*, 2007), using a Gaussian filter to eliminate larger structures in the background, followed by a median filter to remove shot noise (Gonzalez *et al.*, 2003). Remaining interfering bright regions at early time points (e.g., nucleoli, cytoplasmic Cherry-tTA-ER) are cropped from each frame. After these preprocessing steps, a scaled Otsu threshold is applied to each image to identify foreground regions. After loci are segmented in all images, an automated tracking technique is applied to determine temporal associations among segmentation results and define connectivity between successive frames. In the identified region, both red (Cherry) and green (YFP) intensities were reconstructed to individually define Cherry-tTA-ER and YFP-Rpp29 accumulations. Results represent normalized averages of independent data sets. In the first phase, with rapid accumulation, the data were found to fit best to a logistical equation until peak accumulation (T_{peak}), followed by a second phase, in which accumulation remains steady or decreases linearly, quantified by the slope (*m*) from the fit, as follows:

$$F = \frac{A1 - A2}{1 + \left(\frac{x}{x_0}\right)^p} + mx + b \qquad (1)$$

The 95% confidence intervals for the parameter estimates were determined using nlparci MATLAB (Mathworks, Natick, MA). Statistical analysis was done using GraphPad (GraphPad Software, La Jolla, CA) and MATLAB.

Knockdown analyses

Knockdowns were done using shPop4 (Rpp29) (TRCN0000049878; Sigma-Aldrich, St. Louis, MO), shPop1 (TRCN0000049890; Sigma-Aldrich), pLKO.1, and pLKO.1 and shATRX90 (gifts from Roger Everett [University of Glasgow, Glasgow, UK]; Lukashchuk and Everett, 2010; Newhart *et al.* 2012). Lentiviruses were prepared in 293-T cells as previously described (Everett *et al.*, 2008). Briefly, 1×10^6 cells were plated in a 10-cm dish and infected the next day with virus. At 24 h postinfection, cells were

split into 10-cm dishes (1:3). At 48 h, puromycin was added (0.5 µg/ml). At 72 h, cells were harvested for RNA analysis or ChIP.

GST-binding assay

GST-fusion proteins were expressed as previously described (Newhart *et al.*, 2013b). Protein extracts were incubated with Glutathione Superflow beads (Clontech, Mountain View, CA; 1.5–2 h, 4°C with rotation), followed by two washes with resuspension buffer (25 mM Tris, pH 7.5, 0.5 M KCl, 10% glycerol, 5 mM β-mercaptoethanol [β-Me], phenylmethylsulfonyl fluoride). A portion of GST-bound protein beads was saved for SDS–PAGE analysis. Cell lysates were prepared by trypsinizing cells, washing pellets in 1 ml of 1× phosphate-buffered saline (PBS), and resuspending them in 500 µl of nondenaturing lysis buffer (NDLB; 20 mM Tris-HCl, pH 7.4, 2 mM EDTA, 300 mM NaCl, 10% glycerol, 1% NP-40, protease inhibitor cocktail [Sigma-Aldrich]; 30 min, 4°C with rotation). Cell lysates were spun down (14,000 rpm, 10 min, 4°C), and supernatants were collected. Pellets were resuspended in 300 µl of NDLB and sonicated on high for 20 s. Supernatant and sonicated pellet for each individual sample were combined and precleared with 20 µl of prewashed GST beads (1 h, 4°C with rotation). The precleared lysates were spun down, input samples were removed, and the remaining supernatants were incubated with GST-protein bound beads (overnight, 4°C with rotation). Beads were washed three times with resuspension buffer, and then SDS lysis buffer (1% SDS, 10 mM EDTA, 50 mM Tris, pH 8.1) and 3× SDS loading dye (150 mM Tris-HCl, pH 6.8, 6% SDS, 30% glycerol, bromophenol blue, 3% β-Me) were added. Samples were boiled at 95–100°C for 3 min and Western blotted.

To study the effect of RNA and DNA on protein interaction, we treated the cell lysates with different nucleases. For single-stranded RNAs, the cells were lysed in NDLB-A (20 mM Tris-HCl, pH 7.4, 2 mM EDTA, 300 mM NaCl, 10% glycerol, 1% NP-40, protease inhibitor cocktail; 30 min, 4°C with rotation) and treated with 0.01 U/µl RNase A (7.5 U total, 10 min, 37°C). For double-stranded RNA, the cells were lysed in NDLB-B (20 mM Tris-HCl, pH 7.4, 50 mM NaCl, 10% glycerol, 1% NP-40, 1× $MnCl_2$, protease inhibitor cocktail) and treated with 0.01 U/µl shortcut-RNase III (New England Biolabs, Ipswich, MA; 7.5 U total, 10 min, 37°C). The digestion was stopped by adding 1× EDTA to the reaction mixture. Similarly, for DNA, the cells were lysed in NDLB-C (20 mM Tris-HCl, pH 7.4, 100 mM NaCl, 10% glycerol, 1% NP-40, 60 mM $MgCl_2$, 10 mM $CaCl_2$, protease inhibitor cocktail) and treated with 0.01 U/µl RNase-free DNase (Roche Diagnostics, Indianapolis, IN; 7.5 U total, 10 min, 37°C). The reaction was stopped by adding 5 mM EDTA. The cell lysates were then precleared with 20 µl of prewashed GST beads (1 h, 4°C with rotation) and the remaining steps were followed as described.

Immunoblotting

The following antibodies were used: GFP (1:1000; Roche), Flag (1:10,000; M2; Sigma-Aldrich), γ-tubulin (1:500; Sigma-Aldrich), ATRX (1:1000; Santa Cruz Biotechnology, Santa Cruz, CA), and histone H3.3 (1:1000; EMD Millipore, Billerica, MA).

Reverse transcription PCR and quantitative PCR analyses

To collect RNA, cells were trypsinized, pelleted, and lysed in TRIzol (Thermo Fisher Scientific, Waltham, MA); RNA was purified using Direct-zol RNA mini prep kit (Zymo Research, Irvine, CA). Strand-specific quantitative reverse transcription PCR (qRT-PCR) was done as previously described using primers in exon 3 of rabbit β-globin (Newhart *et al.*, 2013b).

The following primer pairs were used to measure Rpp29 and POP1 mRNA levels after knockdown: hRpp29, 5′GGAGCTGCGGCTCTTTGA3′ and 5′GGAGAGGGAGGAAAAGGCTGTA3′; hPOP1, 5′TCGGCAGGGCCTGAGA3′ and 5′GGCAGCAACATGGTTTTCACT3′; and hGAPDH, 5′ATGGAAATCCCATCACCATCTT3′ and 5′CGCCCCACTTGATTTTGG3′.

RNA FISH

RPPH1 and RMRP localization was done using Stellaris RNA FISH probes (LGC Biosearch Technologies, Petaluma, CA) using their standard protocols.

For RPPH1, the probe was composed of the following sequences: 5′ATGAGCTTCCCTCCGCCCTA3′, 5′CACTCAGCTCGTGGCCCCAC3′, 5′ACATGGGAGTGGAGTGACAG3′, 5′TAGTCTCAGACCTTCCCAAG3′, 5′GCTCAGGGAGAGCCCTGTTA3′, 5′GTTCTCTGGGAACTCACCTC3′, 5′TGTTCCAAGCTCCGGCAAAG3′, 5′GAACTCACTTCGCTGGCCGT3′, 5′TTGGGTTATGAGGTCCCCTG 3′, and 5′GGGCGGAGGAGAGTAGTCTG3′.

For RMRP, the probe was composed of the following sequences: 5′CTAGGATACAGGCCTTCAGC3′, 5′AACAGAGTCCTCAGTGTGTA3′, 5′GACTTTCCCCTAGGCGGAAA3′, 5′CACTCTCTGCCCGAGGTCCG3′, 5′GGAATGTCTACGTGCGTATG3′, 5′CGGACTTTGGAGTGGGAAGC3′, 5′CTCAGCGGGATACGCTTCTT3′, 5′AGAGGGAGCTGACGGATGAC3′, 5′GACACGCACTGCCTGCGTAA3′, and 5′TTTTTTACAGCCGCGCTGAG3′.

Native chromatin immunoprecipitation

Native chromatin immunoprecipitation was done in HeLa HI 1-1/H3.3-YFP cells as previously described (Newhart *et al.*, 2012) using 2 µg of anti-GFP antibody (Roche) and protein A+G agarose/salmon sperm DNA (Millipore, Temecula, CA).

High-salt histone extraction

High-salt histone extraction was done as previously described (Shechter *et al.*, 2007). To isolate nuclei, control and shRNA Rpp29+ATRX cells were typsinized from culture dishes, and ~(1.5–2) × 10^6 cells were washed with 1× PBS, resuspended in 500 µl of extraction buffer (EB; 10 mM 4-(2-hydroxyethyl)-1-piperazineethanesulfonic acid, pH 7.9, 10 mM KCl, 1.5 mM $MgCl_2$, 0.34 M sucrose, and 10% glycerol) plus 0.2% NP-40, incubated on ice for 10 min with occasional rotating, and centrifuged to pellet nuclei (5 min, 6500 × *g* at 4°C). Nuclei were washed with EB and resuspended in 200 µl of no-salt buffer (3 mM EDTA, 0.2 mM ethylene glycol tetraacetic acid), and inputs were collected. To extract unincorporated histones, nuclei were vortexed intermittently for 1 min and incubated with rotation (30 min, 4°C). Nuclei were divided into three equal fractions and pelleted (5 min, 6500 × *g*, 4°C), and supernatants were collected and combined (i.e., unincorporated histones). The pellets were then resuspended in 80 µl of salt solubilization buffer (50 mM Tris-Cl, pH 8.0, 0.05% NP-40) containing 0, 1, or 2 N NaCl, vortexed for 2 min, and incubated with rotation (30 min, 4°C). The samples were centrifuged (10 min, 16,000 × *g*, 4°C), and supernatants were collected. Immunoblot band intensity was quantified by densitometry using ImageJ software (version 1.48; National Institutes of Health, Bethesda, MD).

Fluorescence recovery after photobleaching

HeLa HI 1-1 cells stably expressing H3.3-YFP and infected with control (pLKO.1) and/or Rpp29+ATRX shRNAs for 72 h were grown in 35-mm glass-bottom dishes (CELLview; Greiner Bio-One, Monroe, NC). Photobleaching was done with a Leica SP5II confocal laser-scanning microscope (Leica Microsystems, Buffalo Grove, IL) with a

heated and humidified environmental chamber (37°C, 5% CO_2) and a 63× oil objective lens (numerical aperture 1.4) with 6× zoom. The 514-nm argon laser line (50% power) was used for imaging, with bleaching done at 100% and measurements at 3% of available laser power. Airy unit was set at 2, and bidirectional scanning was done at 1400 Hz. Long, 10-min time-course experiments were conducted with 20 prebleach frames set to minimum intervals to get an intensity baseline, followed by six bleach frames at a 0.189-s read rate, followed by 120 frames at 5-s intervals. The photomultiplier tube detector was set at 524–600 nm and gain at 670. Images were captured with three nuclei/field; two were bleached, and one was used as a control for system bleaching. Data were collected using the FRAP Wizard macro in LAS software using a 3-μm circle and exported to ImagePro Plus (MediaCybernetics, Rockville, MD) to set a track accounting for movement of the bleached area over time. The measured ROI was standardized to a 1-μm circle. Four ROIs were measured per field: two cells with one bleach spot, a spot in an unbleached nucleus, and the adjacent region of black background (McNally, 2008).

ACKNOWLEDGMENTS

We thank Sidney Altman, Roger Everett, and Sui Huang for reagents, Sylvie Shaffer for her artistic contributions to the model, and Matthew Weitzman for helpful discussions. This work was funded by start-up funding from the Wistar Institute and grants from the Arnold and Mabel Beckman Foundation, the Mallinckrodt Foundation, the Emerald Foundation, the March of Dimes Basil O'Connor Award, the National Institutes of Health (R01 GM 093000-02), and the Wistar Cancer Center Core Grant Facilities (P30 CA10815): Genomics, Protein Expression and Imaging.

REFERENCES

Banaszynski LA, Wen D, Dewell S, Whitcomb SJ, Lin M, Diaz N, Elsasser SJ, Chapgier A, Goldberg AD, Canaani E, *et al.* (2013). Hira-dependent histone H3.3 deposition facilitates PRC2 recruitment at developmental loci in ES cells. Cell 155, 107–120.

Bender S, Tang Y, Lindroth AM, Hovestadt V, Jones DT, Kool M, Zapatka M, Northcott PA, Sturm D, Wang W, *et al.* (2013). Reduced H3K27me3 and DNA hypomethylation are major drivers of gene expression in K27M mutant pediatric high-grade gliomas. Cancer Cell 24, 660–672.

Bernstein BE, Mikkelsen TS, Xie X, Kamal M, Huebert DJ, Cuff J, Fry B, Meissner A, Wernig M, Plath K, *et al.* (2006). A bivalent chromatin structure marks key developmental genes in embryonic stem cells. Cell 125, 315–326.

Beronja S, Janki P, Heller E, Lien WH, Keyes BE, Oshimori N, Fuchs E (2013). RNAi screens in mice identify physiological regulators of oncogenic growth. Nature 501, 185–190.

Bhavsar RB, Makley LN, Tsonis PA (2010). The other lives of ribosomal proteins. Hum Genomics 4, 327–344.

Bower K, Napier CE, Cole SL, Dagg RA, Lau LM, Duncan EL, Moy EL, Reddel RR (2012). Loss of wild-type ATRX expression in somatic cell hybrids segregates with activation of Alternative Lengthening of Telomeres. PLoS One 7, e50062.

Chan KM, Fang D, Gan H, Hashizume R, Yu C, Schroeder M, Gupta N, Mueller S, James CD, Jenkins R, *et al.* (2013). The histone H3.3K27M mutation in pediatric glioma reprograms H3K27 methylation and gene expression. Genes Dev 27, 985–990.

Chen D, Huang S (2001). Nucleolar components involved in ribosome biogenesis cycle between the nucleolus and nucleoplasm in interphase cells. J Cell Biol 153, 169–176.

Clynes D, Jelinska C, Xella B, Ayyub H, Taylor S, Mitson M, Bachrati CZ, Higgs DR, Gibbons RJ (2014). ATRX dysfunction induces replication defects in primary mouse cells. PLoS One 9, e92915.

Delbarre E, Ivanauskiene K, Kuntziger T, Collas P (2012). DAXX-dependent supply of soluble (H3.3-H4) dimers into PML bodies pending deposition into chromatin. Genome Res 23, 440–451.

Delbarre E, Jacobsen BM, Reiner AH, Sorensen AL, Kuntziger T, Collas P (2010). Chromatin environment of histone variant H3.3 revealed by quantitative imaging and genome-scale chromatin and DNA immunoprecipitation. Mol Biol Cell 21, 1872–1884.

Drane P, Ouararhni K, Depaux A, Shuaib M, Hamiche A (2010). The death-associated protein DAXX is a novel histone chaperone involved in the replication-independent deposition of H3.3. Genes Dev 24, 1253–1265.

Elsasser SJ, Huang H, Lewis PW, Chin JW, Allis CD, Patel DJ (2012). DAXX envelops a histone H3.3-H4 dimer for H3.3-specific recognition. Nature 491, 560–565.

Elsasser SJ, Noh KM, Diaz N, Allis CD, Banaszynski LA (2015). Histone H3.3 is required for endogenous retroviral element silencing in embryonic stem cells. Nature 522, 240–244.

Episkopou H, Draskovic I, Van Beneden A, Tilman G, Mattiussi M, Gobin M, Arnoult N, Londono-Vallejo A, Decottignies A (2014). Alternative Lengthening of Telomeres is characterized by reduced compaction of telomeric chromatin. Nucleic Acids Res 42, 4391–4405.

Everett RD, Parada C, Gripon P, Sirma H, Orr A (2008). Replication of ICP0-null mutant herpes simplex virus type 1 is restricted by both PML and Sp100. J Virol 82, 2661–2672.

Filipescu D, Szenker E, Almouzni G (2013). Developmental roles of histone H3 variants and their chaperones. Trends Genet 29, 630–640.

Flynn RL, Cox KE, Jeitany M, Wakimoto H, Bryll AR, Ganem NJ, Bersani F, Pineda JR, Suva ML, Benes CH, *et al.* (2015). Alternative lengthening of telomeres renders cancer cells hypersensitive to ATR inhibitors. Science 347, 273–277.

Fulka H, Langerova A (2014). The maternal nucleolus plays a key role in centromere satellite maintenance during the oocyte to embryo transition. Development 141, 1694–1704.

Garrick D, Fiering S, Martin DI, Whitelaw E (1998). Repeat-induced gene silencing in mammals. Nat Genet 18, 56–59.

Goldberg AD, Banaszynski LA, Noh KM, Lewis PW, Elsaesser SJ, Stadler S, Dewell S, Law M, Guo X, Li X, *et al.* (2010). Distinct factors control histone variant H3.3 localization at specific genomic regions. Cell 140, 678–691.

Gonzalez RC, Woods RE, Eddins SL (2003). Digital Image Processing Using MATLAB, Upper Saddle River, NJ: Pearson Prentice Hall.

Hayashihara K, Uchiyama S, Shimamoto S, Kobayashi S, Tomschik M, Wakamatsu H, No D, Sugahara H, Hori N, Noda M, *et al.* (2010). The middle region of an HP1-binding protein, HP1-BP74, associates with linker DNA at the entry/exit site of nucleosomal DNA. J Biol Chem 285, 6498–6507.

He Q, Kim H, Huang R, Lu W, Tang M, Shi F, Yang D, Zhang X, Huang J, Liu D, Songyang Z (2015). The Daxx/Atrx complex protects tandem repetitive elements during DNA hypomethylation by promoting H3K9 trimethylation. Cell Stem Cell 17, 273–286.

Heaphy CM, de Wilde RF, Jiao Y, Klein AP, Edil BH, Shi C, Bettegowda C, Rodriguez FJ, Eberhart CG, Hebbar S, *et al.* (2011). Altered telomeres in tumors with ATRX and DAXX mutations. Science 333, 425.

Jacobson MR, Cao LG, Taneja K, Singer RH, Wang YL, Pederson T (1997). Nuclear domains of the RNA subunit of RNase P. J Cell Sci 110, 829–837.

Jang CW, Shibata Y, Starmer J, Yee D, Magnuson T (2015). Histone H3.3 maintains genome integrity during mammalian development. Genes Dev 29, 1377–1392.

Janicki SM, Tsukamoto T, Salghetti SE, Tansey WP, Sachidanandam R, Prasanth KV, Ried T, Shav-Tal Y, Bertrand E, Singer RH, Spector DL (2004). From silencing to gene expression: real-time analysis in single cells. Cell 116, 683–698.

Jarrous N, Reiner R, Wesolowski D, Mann H, Guerrier-Takada C, Altman S (2001). Function and subnuclear distribution of Rpp21, a protein subunit of the human ribonucleoprotein ribonuclease P. RNA 7, 1153–1164.

Jarrous N, Wolenski JS, Wesolowski D, Lee C, Altman S (1999). Localization in the nucleolus and coiled bodies of protein subunits of the ribonucleoprotein ribonuclease P. J Cell Biol 146, 559–572.

Khanova E, Esakova O, Perederina A, Berezin I, Krasilnikov AS (2012). Structural organizations of yeast RNase P and RNase MRP holoenzymes as revealed by UV-crosslinking studies of RNA-protein interactions. RNA 18, 720–728.

Kimura H, Cook PR (2001). Kinetics of core histones in living human cells: little exchange of H3 and H4 and some rapid exchange of H2B. J Cell Biol 153, 1341–1353.

Kiss T, Fayet E, Jady BE, Richard P, Weber M (2006). Biogenesis and intranuclear trafficking of human box C/D and H/ACA RNPs. Cold Spring Harb Symp Quant Biol 71, 407–417.

Levy MA, Kernohan KD, Jiang Y, Berube NG (2015). ATRX promotes gene expression by facilitating transcriptional elongation through guanine-rich coding regions. Hum Mol Genet 24, 1824–1835.
Lewis PW, Elsaesser SJ, Noh KM, Stadler SC, Allis CD (2010). Daxx is an H3.3-specific histone chaperone and cooperates with ATRX in replication-independent chromatin assembly at telomeres. Proc Natl Acad Sci USA 107, 14075–14080.
Lewis PW, Muller MM, Koletsky MS, Cordero F, Lin S, Banaszynski LA, Garcia BA, Muir TW, Becher OJ, Allis CD (2013). Inhibition of PRC2 activity by a gain-of-function H3 mutation found in pediatric glioblastoma. Science 340, 857–861.
Lindroth AM, Plass C (2013). Recurrent H3.3 alterations in childhood tumors. Nat Genet 45, 1413–1414.
Loppin B, Bonnefoy E, Anselme C, Laurencon A, Karr TL, Couble P (2005). The histone H3.3 chaperone HIRA is essential for chromatin assembly in the male pronucleus. Nature 437, 1386–1390.
Lovejoy CA, Li W, Reisenweber S, Thongthip S, Bruno J, de Lange T, De S, Petrini JH, Sung PA, Jasin M, *et al.* (2012). Loss of ATRX, genome instability, and an altered DNA damage response are hallmarks of the alternative lengthening of telomeres pathway. PLoS Genet 8, e1002772.
Luger K, Mader AW, Richmond RK, Sargent DF, Richmond TJ (1997). Crystal structure of the nucleosome core particle at 2.8 A resolution. Nature 389, 251–260.
Lukashchuk V, Everett RD (2010). Regulation of ICP0-null mutant herpes simplex virus type 1 infection by ND10 components ATRX and hDaxx. J Virol 84, 4026–4040.
Martin C, Beaujean N, Brochard V, Audouard C, Zink D, Debey P (2006). Genome restructuring in mouse embryos during reprogramming and early development. Dev Biol 292, 317–332.
Marvin MC, Clauder-Munster S, Walker SC, Sarkeshik A, Yates JR 3rd, Steinmetz LM, Engelke DR (2011). Accumulation of noncoding RNA due to an RNase P defect in Saccharomyces cerevisiae. RNA 17, 1441–1450.
Marvin MC, Engelke DR (2009). Broadening the mission of an RNA enzyme. J Cell Biochem 108, 1244–1251.
McBurney MW, Mai T, Yang X, Jardine K (2002). Evidence for repeat-induced gene silencing in cultured mammalian cells: inactivation of tandem repeats of transfected genes. Exp Cell Res 274, 1–8.
McNally JG (2008). Quantitative FRAP in analysis of molecular binding dynamics in vivo. Methods Cell Biol 85, 329–351.
Meshorer E, Yellajoshula D, George E, Scambler PJ, Brown DT, Misteli T (2006). Hyperdynamic plasticity of chromatin proteins in pluripotent embryonic stem cells. Dev Cell 10, 105–116.
Michel R, Steinmeyer R, Falk M, Harms GS (2007). A new detection algorithm for image analysis of single, fluorescence-labeled proteins in living cells. Microsc Res Tech 70, 763–770.
Molla-Herman A, Valles AM, Ganem-Elbaz C, Antoniewski C, Huynh JR (2015). tRNA processing defects induce replication stress and Chk2-dependent disruption of piRNA transcription. EMBO J 34, 3009–3027.
Natrajan R, Mackay A, Wilkerson PM, Lambros MB, Wetterskog D, Arnedos M, Shiu KK, Geyer FC, Langerod A, Kreike B, *et al.* (2012). Functional characterization of the 19q12 amplicon in grade III breast cancers. Breast Cancer Res 14, R53.
Newhart A, Janicki SM (2014). Seeing is believing: visualizing transcriptional dynamics in single cells. J Cell Physiol 229, 259–265.
Newhart A, Negorev DG, Rafalska-Metcalf IU, Yang T, Maul GG, Janicki SM (2013a). Sp100A promotes chromatin decondensation at a cytomegalovirus-promoter-regulated transcription site. Mol Biol Cell 24, 1454–1468.
Newhart A, Rafalska-Metcalf IU, Yang T, Joo LM, Powers SL, Kossenkov AV, Lopez-Jones M, Singer RH, Showe LC, Skordalakes E, Janicki SM (2013b). Single cell analysis of RNA-mediated histone H3.3 recruitment to a cytomegalovirus promoter-regulated transcription site. J Biol Chem 288, 19882–19899.
Newhart A, Rafalska-Metcalf IU, Yang T, Negorev DG, Janicki SM (2012). Single-cell analysis of Daxx and ATRX-dependent transcriptional repression. J Cell Sci 125, 5489–5501.
O'Sullivan RJ, Arnoult N, Lackner DH, Oganesian L, Haggblom C, Corpet A, Almouzni G, Karlseder J (2014). Rapid induction of alternative lengthening of telomeres by depletion of the histone chaperone ASF1. Nat Struct Mol Biol 21, 167–174.
Probst AV, Santos F, Reik W, Almouzni G, Dean W (2007). Structural differences in centromeric heterochromatin are spatially reconciled on fertilisation in the mouse zygote. Chromosoma 116, 403–415.
Rafalska-Metcalf IU, Janicki SM (2013). Preparation of cell lines for single-cell analysis of transcriptional activation dynamics. Methods Mol Biol 977, 249–258.
Rafalska-Metcalf IU, Powers SL, Joo LM, LeRoy G, Janicki SM (2010). Single cell analysis of transcriptional activation dynamics. PLoS One 5, e10272.
Reiner R, Alfiya-Mor N, Berrebi-Demma M, Wesolowski D, Altman S, Jarrous N (2011). RNA binding properties of conserved protein subunits of human RNase P. Nucleic Acids Res 39, 5704–5714.
Reuss DE, Sahm F, Schrimpf D, Wiestler B, Capper D, Koelsche C, Schweizer L, Korshunov A, Jones DT, Hovestadt V, *et al.* (2014). ATRX and IDH1-R132H immunohistochemistry with subsequent copy number analysis and IDH sequencing as a basis for an "integrated" diagnostic approach for adult astrocytoma, oligodendroglioma and glioblastoma. Acta Neuropathol 129, 133–146.
Sadic D, Schmidt K, Groh S, Kondofersky I, Ellwart J, Fuchs C, Theis FJ, Schotta G (2015). Atrx promotes heterochromatin formation at retrotransposons. EMBO Rep 16, 836–850.
Santenard A, Ziegler-Birling C, Koch M, Tora L, Bannister AJ, Torres-Padilla ME (2010). Heterochromatin formation in the mouse embryo requires critical residues of the histone variant H3.3. Nat Cell Biol 12, 853–862.
Sarma K, Cifuentes-Rojas C, Ergun A, Del Rosario A, Jeon Y, White F, Sadreyev R, Lee JT (2014). ATRX directs binding of PRC2 to Xist RNA and Polycomb targets. Cell 159, 869–883.
Shechter D, Dormann HL, Allis CD, Hake SB (2007). Extraction, purification and analysis of histones. Nat Protoc 2, 1445–1457.
Talbert PB, Henikoff S (2010). Histone variants—ancient wrap artists of the epigenome. Nat Rev Mol Cell Biol 11, 264–275.
Tessarz P, Santos-Rosa H, Robson SC, Sylvestersen KB, Nelson CJ, Nielsen ML, Kouzarides T (2013). Glutamine methylation in histone H2A is an RNA-polymerase-I-dedicated modification. Nature 505, 564–568.
Torres-Padilla ME, Bannister AJ, Hurd PJ, Kouzarides T, Zernicka-Goetz M (2006). Dynamic distribution of the replacement histone variant H3.3 in the mouse oocyte and preimplantation embryos. Int J Dev Biol 50, 455–461.
Tsukamoto T, Hashiguchi N, Janicki SM, Tumbar T, Belmont AS, Spector DL (2000). Visualization of gene activity in living cells. Nat Cell Biol 2, 871–878.
Udugama M, Chang FT, Chan FL, Tang MC, Pickett HA, McGhie JD, Mayne L, Collas P, Mann JR, Wong LH (2015). Histone variant H3.3 provides the heterochromatic H3 lysine 9 tri-methylation mark at telomeres. Nucleic Acids Res 43, 10227–10237.
Venneti S, Garimella MT, Sullivan LM, Martinez D, Huse JT, Heguy A, Santi M, Thompson CB, Judkins AR (2013). Evaluation of histone 3 lysine 27 trimethylation (H3K27me3) and enhancer of Zest 2 (EZH2) in pediatric glial and glioneuronal tumors shows decreased H3K27me3 in H3F3A K27M mutant glioblastomas. Brain Pathol 23, 558–564.
Voon HP, Hughes JR, Rode C, De La Rosa-Velazquez IA, Jenuwein T, Feil R, Higgs DR, Gibbons RJ (2015). ATRX plays a key role in maintaining silencing at interstitial heterochromatic loci and imprinted genes. Cell Rep 11, 405–418.
Wilson RC, Bohlen CJ, Foster MP, Bell CE (2006). Structure of Pfu Pop5, an archaeal RNase P protein. Proc Nat Acad Sci USA 103, 873–878.
Wong LH, McGhie JD, Sim M, Anderson MA, Ahn S, Hannan RD, George AJ, Morgan KA, Mann JR, Choo KH (2010). ATRX interacts with H3.3 in maintaining telomere structural integrity in pluripotent embryonic stem cells. Genome Res 20, 351–360.
Wong LH, Ren H, Williams E, McGhie J, Ahn S, Sim M, Tam A, Earle E, Anderson MA, Mann J, Choo KH (2009). Histone H3.3 incorporation provides a unique and functionally essential telomeric chromatin in embryonic stem cells. Genome Res 19, 404–414.
Wrzeszczynski KO, Varadan V, Byrnes J, Lum E, Kamalakaran S, Levine DA, Dimitrova N, Zhang MQ, Lucito R (2011). Identification of tumor suppressors and oncogenes from genomic and epigenetic features in ovarian cancer. PLoS One 6, e28503.
Xu Y, Oruganti SV, Gopalan V, Foster MP (2012). Thermodynamics of coupled folding in the interaction of archaeal RNase P proteins RPP21 and RPP29. Biochemistry 51, 926–935.
Yang JH, Song Y, Seol JH, Park JY, Yang YJ, Han JW, Youn HD, Cho EJ (2011). Myogenic transcriptional activation of MyoD mediated by replication-independent histone deposition. Proc Natl Acad Sci USA 108, 85–90.